

Photometric determination of the mass accretion rates of pre-main sequence stars. III. Results in the Large Magellanic Cloud

L. Spezzi^{1*}†, G. De Marchi¹, N. Panagia^{2,3,4}, A. Sicilia-Aguilar^{5,6} and B. Ercolano^{7,8}

¹European Space Agency (ESTEC), PO Box 299, 2200 AG Noordwijk, The Netherlands

²Space Telescope Science Institute, 3700 San Martin Drive, Baltimore, MD 21218

³INAFCT, Osservatorio Astrofisico di Catania, Via S. Sofia 78, I-95123 Catania, Italy

⁴Supernova Limited, OYV No. 131, Northsound Rd., Virgin Gorda, British Virgin Islands

⁵Max-Planck-Institut für Astronomie, Königstuhl 17, 69117 Heidelberg, Germany

⁶Departamento de Física Teórica, Universidad Autónoma de Madrid, Cantoblanco 28049, Madrid, Spain

⁷Ludwig-Maximilians-Universität, University Observatory Munich, Scheinerstr. 1, D-81679 München, Germany

⁸Cluster of Excellence “Origin and Structure of the Universe”, Boltzmannstr.2, 85748 Garching, Germany

Accepted 2011 YYYYYY xx. Received 2011 XXXXX yy; in original form 2011 June 27

ABSTRACT

We present a multi-wavelength study of three star forming regions, spanning the age range 1–14 Myr, located between the 30 Doradus complex and supernova SN1987A in the Large Magellanic Cloud (LMC). We reliably identify about 1000 pre-main sequence (PMS) star candidates actively undergoing mass accretion and estimate their stellar properties and mass accretion rate (\dot{M}). Our measurements represent the largest \dot{M} dataset of low-metallicity stars presented so far. As such, they offer a unique opportunity to study on a statistical basis the mass accretion process in the LMC and, more in general, the evolution of the mass accretion process around low-metallicity stars. We find that the typical \dot{M} of PMS stars in the LMC is higher than for galactic PMS stars of the same mass, independently of their age. Taking into account the caveats of isochronal age and \dot{M} estimates, the difference in \dot{M} between the LMC and our Galaxy appears to be about an order of magnitude. We review the main mechanisms of disk dispersal and find indications that typically higher \dot{M} are to be expected in low-metallicity environments. However, many issues of this scenario need to be clarified by future observations and modeling. We also find that, in the mass range 1–2 M_{\odot} , the \dot{M} of PMS stars in the LMC increases with stellar mass as $\dot{M} \propto M_{\star}^b$ with $b \approx 1$, i.e. slower than the second power law found for galactic PMS stars in the same mass regime.

Key words: Galaxies: Magellanic Clouds - stars: formation - stars: pre-main-sequence - stars: circumstellar matter

1 INTRODUCTION

The mass accretion rate (\dot{M}) of young stars is a key parameter to constrain the models of both star and planet formation. \dot{M} is an indicator of the presence of gas, and hence dust, in the inner circumstellar disk and, as such, it is affected by the disk structure and evolution as well as by the formation and migration of planets (see, e.g., Calvet et al. 2000). Thus, it is of particular interest to determine the evolution of \dot{M} as a star approaches its main sequence, whether \dot{M} and stellar mass are correlated, and whether it is affected by the specific conditions of a given star formation event, such as the chemical composition and density of the parent molecular cloud, by the proximity of hot massive stars, etc. The measure of \dot{M} generally relies on the study of continuum veiling, UV excess emission or profile/intensity of emission lines (usually $H\alpha$, $Pa\beta$ or

$B\gamma$), which requires medium to high resolution spectroscopy of individual young objects. As a result, the data collected so far are limited to nearby ($d \lesssim 1\text{--}2$ kpc) star forming regions. These data indicate that \dot{M} is a decreasing function of stellar age (Muzerolle et al. 2000; Sicilia-Aguilar et al. 2005, 2006, 2010; Fedele et al. 2010), in line with the expected evolution of viscous discs (Hartmann et al. 1998), and is roughly proportional to the second power of the stellar mass (Muzerolle et al. 2005; Natta et al. 2006; Sicilia-Aguilar et al. 2006). However, the detection limits and the difficulty of measuring very small \dot{M} do not allow us to rule out detection/selection thresholds as responsible of this trend (see, e.g., Clarke & Pringle 2006). Moreover, the spread of the \dot{M} data exceeds 2 dex at any given age. Several facets of the mass accretion process appear to contribute to this spread: i) at any age, disks in different evolutionary stages coexist in the same star forming region (see, e.g., Harvey et al. 2007; Alcalá et al. 2008; Merín et al. 2008); ii) \dot{M} depends on the disk mass and, hence, on the mass of the forming star (White & Hillenbrand 2004; Alcalá et al. 2008; Kim et al. 2009);

* E-mail: lspezzi@rssd.esa.int

† Facilities: HST (WFPC2)

iii) the accretion process in young stars, and the accretion-related emission lines, are subject to variations on a timescale of a few hours to years or even decades (Herbst 1986; Hartigan et al. 1991; Nguyen et al. 2009). Another limitation of the galactic objects for which \dot{M} measurements are currently available is that they have essentially solar metallicity (e.g. Padgett 1996), because they are located in nearby star forming regions.

In the past two decades, many authors have demonstrated the potential of deep Hubble Space Telescope (HST) optical imaging for star formation studies. Recently, De Marchi et al. (2010) (hereafter Paper I) presented a novel method to identify pre-main sequence (PMS) objects actively undergoing mass accretion and determine their \dot{M} . This method relies solely on HST imaging, which can be easily obtained for a large number of PMS stars at once and for distant star forming regions, well beyond a few kpc and with different metallicity, allowing us to overcome some of the limitations affecting techniques based on spectroscopy. This method has been already adapted to the Wide Field Camera (WFC) of the Isaac Newton Telescope (INT) and is being used within the frame of INT Photometric H-Alpha Survey (IPHAS), a 1800 deg² survey of the Northern Galactic Plane aiming at reliably select classical T Tauri stars and constrain their mass accretion rates (Barentsen et al. 2011). We have now started a pilot project aiming at applying this technique to the existing and extensive HST photometry of star-forming regions in the Milky Way (MW) and the MCs. In this paper we present the results of this study in the Large Magellanic Cloud (LMC).

Because of its relative proximity (51.4±1.2 kpc; Panagia 1991; Panagia et al. 1991) and low-metal content ($Z=0.007$; Maeder et al. 1999, and references therein), the LMC is a very interesting test-case for star formation studies and, specifically, for mass accretion studies, because it offers a unique opportunity to study a resolved accreting stellar population in an environment with a chemical composition different from the MW ($Z\approx 0.018$; see Esteban & Peimbert 1995).

Investigating the \dot{M} vs. metallicity dependency is of special interest for several reasons:

(i) The time-scale of the mass accretion process is strongly connected with the disk lifetime, which has been poorly studied in low-metallicity environments (see, e.g., Yasui et al. 2009). Thus, studying the \dot{M} evolution might help clarifying how different disk dispersal mechanisms act at lower-metallicity.

(ii) Low-metallicity disks can be used as a benchmark for evolved solar-metallicity disks, where dust grains may have suffered strong coagulation (see Ercolano & Clarke 2010, and discussion at the Ringberg Accretion Workshop 2011¹).

(iii) The evolution of \dot{M} is affected by possible planet formation in the disk and, hence, it might provide new important clues on the so called “planet-metallicity correlation”. The probability of a star hosting a planet appears to increase with stellar metallicity (Gonzalez 1997; Fischer & Valenti 2005; Santos et al. 2003). However, a few planets have been found around metal-poor stars (see, e.g. Santos et al. 2007; Setiawan et al. 2003, 2010) and the frequency of planets around metal-poor stars compared to solar-metallicity stars is still uncertain. Thus, the “planet-metallicity correlation” could be a simple selection effect. Indeed, surveys for extra-solar planets are mainly based on the radial velocity (RV) method (Mayor & Queloz 1995; Marcy & Butler 1998, and references therein) and RV variations are much harder to detect in stel-

lar spectra presenting few metallic lines. As a consequence, only a few planets have been found around very metal poor stars and, because of this indication, metal-poor stars are systematically excluded from RV surveys.

This paper is organized as follows: Sect. 2 describes the selection of the LMC fields among those available in the HST archive and the data reduction. In Sect. 3 we apply the method described in Paper I to select PMS objects and calculate their \dot{M} . The results are presented in Sect. 4 -8, where in particular we discuss the mass dependency of \dot{M} , its evolution and metallicity dependency in relation with disk dispersal mechanisms such as planet formation and disk photo-evaporation. The conclusions of this work are given in Sect. 9.

2 DATA SAMPLE

We selected three 162”×162” areas in the LMC located between the 30 Doradus star forming complex and supernova SN1987A (Figure 1). All fields were selected from the HST Archival Pure Parallel Project²; the proposal ID and Principal Investigator (PI) for each dataset are reported in Table 1. The observations were performed from February 1999 to November 2003 with the Wide Field Planetary Camera 2 (WFPC2) of the HST using the F606W (V), F656N (H α) and F814W (I) filters. The three fields were selected following two basic criteria: i) exposure time long enough to allow the detection of objects down to 0.8-1 M_⊙ at the distance of LMC in the three filters; ii) different environmental conditions, such as vicinity to OB stars and amount of interstellar gas and dust, in order to study the behavior of \dot{M} in star-forming regions with different properties.

The basic data set used for this paper was retrieved from the HST archive at the Canadian Astronomy Data Centre (CADC). The sources identification and photometry was performed on the stacked images using the SExtractor 2.5 tool by Bertin & Arnouts (1996). SExtractor exploits the aperture photometry technique, which is the fastest and best approach for not-crowded fields as those considered here, and the background is locally estimated in an annulus surrounding the star. Following the prescriptions of the HST Data Handbook for the WFPC2 (Baggett et al. 2002), we adopted a 0.5 arcsec aperture radius for magnitude extraction and then calibrated the instrumental magnitudes to the VEGA-MAG photometric system using the zeropoints listed in Table 5.1 of the handbook. The SExtractor morphological parameter “extraction flag” (FLAGS) was used to clean the catalogs from spurious detections, such as saturated or truncated sources too close to the image boundaries, etc. Table 1 summarizes, for each of the three fields, the total exposure time, the saturation limit and the limiting magnitude achieved at the 10 σ level in each filter. The exposure times are not uniform across our dataset, producing different saturation limits and limiting magnitudes for each filter/region. Considering the distance to the LMC (~50 kpc) and the typical age of our regions (Table 4) and using the evolutionary models for PMS stars by Tognelli et al. (2011) for the metallicity of the LMC ($Z=0.007$; Maeder et al. 1999, and references therein), we concluded that our observations are complete above 1 M_⊙ for the three regions in all the filters. Thus, in Sect. 5-6 we will limit our analysis to the mass range 1-2 M_⊙.

In addition to the above fields, we have used WFPC2 photometry of a field around supernova SN1987A studied by

¹ <http://accretion2011.mpe.mpg.de/index.php>

² See <http://archive.stsci.edu/prepds/appp> for details.

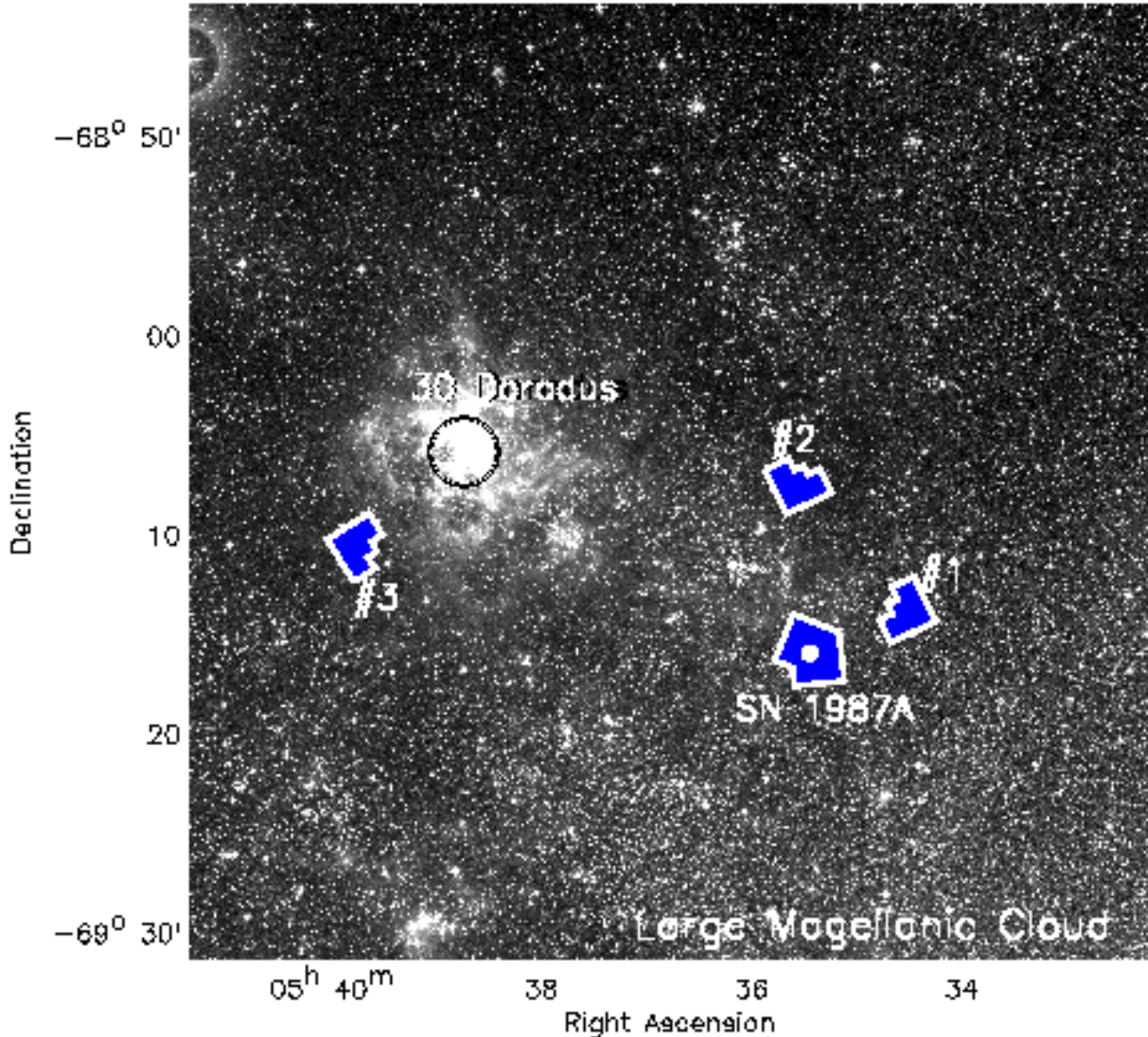


Figure 1. R-band image of a $40' \times 40'$ area in the LMC from the Sloan Digital Sky Survey. The polygons display the four regions observed with HST/WFPC2 analyzed in this paper. The position of 30 Doradus star-burst cluster and the supernova SN1987A are also indicated.

Romaniello (1998), Panagia et al. (2000) and Romaniello et al. (2002). These observations are centered at R.A. = $5^h 35^m 28^s$ and Dec. = $-69^{\text{deg}} 16^m 12^s$ and cover a field of 9.16 square arcmin. The mass accretion rate for the PMS stars in this field were already derived in Paper I.

3 SELECTION OF PMS STARS

We select PMS stars in each field and determine their mass accretion rates using narrow-band $H\alpha$ (f656n) and broad-band V (f606w) and I (f814w) dereddened photometry. In the following sections we describe the main steps of our selection procedure. For a more detailed description of this method we refer the reader to Paper I.

3.1 Reddening

From a visual inspection of the images, we find evidence of patchy nebulosity in our fields and we therefore can expect a certain amount of differential reddening.

To test this hypothesis, we divided each field in 22 regions, each $32'' \times 32''$ in size, and obtain the V vs. V-I colour-magnitude diagram (CMD) for each sub-image. We used the zero age main sequence (ZAMS) by Marigo et al. (2008) for the metallicity of the LMC as the reference unreddened CMD (Figure 2). The ZAMS was shifted to the distance of the LMC and reddened by the amount corresponding to the intervening absorption along the line of sight due to the Milky Way, which Fitzpatrick & Savage (1984) quantified in $A_V = 0.22$, in turn corresponding to $E(V-I) = 0.1$.

Within each sub-image we derived for all stars a single value the reddening relative to the ZAMS in the following way. For each star with $18 < V < 24$ and $0 < V-I < 1.3$, we calculated the distance from the ZAMS along the reddening vector, defined by the extinction

Field	HST proposal ID	PI	RAJ2000 _{center} (hh:mm:ss)	DECJ2000 _{center} (dd:mm:ss)	Filter	T _{exp} (min)	Mag Sat.	Mag 10 σ
#1	8059	Stefano Casertano	05:34:34.03	-69:14:01.50	F606W	17	17.00	24.30
					F656N	73	15.00	21.00
					F814W	39	17.00	23.80
#2	9634	James Rhoads	05:35:34.93	-69:07:32.36	F606W	49	17.50	25.20
					F656N	68	15.50	21.30
					F814W	35	16.00	24.30
#3	8059	Stefano Casertano	05:39:40.57	-69:10:48.43	F606W	8	16.00	23.80
					F656N	57	14.30	20.00
					F814W	15	15.50	23.50

Table 1. HST proposal ID, PI name, total exposure time, saturation limit and limiting magnitude at 10 σ level for the three HST-WFPC2 pointings used in this paper.

law as measured specifically in the LMC by Scuderi et al. (1996). Each one of these distances is the resultant of two components, namely E(V-I) along the abscissa and A_V along the ordinates. We then looked at the distribution of A_V values inside each cell and took the 17th percentile as a conservative lower limit to the value of A_V for the whole cell (see example in Figure 3). If the reddening distribution were Gaussian, this would correspond to 1σ . The purpose of this approach is to minimize the number of stars that after the correction become bluer than the ZAMS and to keep them to a fraction compatible with our photometric uncertainties. This choice ensures that we are not overestimating the reddening correction for the majority of the stars in the field. It also avoids an improper overestimation of the ages due to an excessive reddening correction (see reddening lines in Figure 2).

The relative A_V values of the sub-images span a range of 0.4 mag in our field #1, 0.6 mag in our field #2 and 1.2 mag in our field #3. Thus, differential reddening is more significant in field #3, which is indeed the closest one to the 30 Doradus star-burst cluster and is still associated with conspicuous gaseous/dusty nebosity (Figure 9).

We correct the magnitudes of each source in each filter assuming the A_V estimated for the relative sub-image and the extinction law by Scuderi et al. (1996). This statistical method, though providing only a rough estimate of the visual extinction toward the given source, is suitable for our purposes. Indeed, in Paper I we have demonstrated that for an average LMC star-forming region omitting the extinction correction would result in a 10% overestimate of the mass accretion rate. This error, albeit systematic, is smaller than most other systematic uncertainties and comparable to the measurement errors.

3.2 Selection of stars with H α excess emission

We select PMS stars on the basis of their H α emission line (White & Basri 2003). The traditional approach to search for H α emitters is based on the use of the R-band magnitude as an indicator of the level of the photospheric continuum near the H α line, so that stars with strong H α emission will have a large $R - H\alpha$ color. Since we do not dispose of R-band photometry for our fields, we use measurements in the neighboring V and I bands, following the approach described in Paper I.

Figure 4 (top panel) shows, as an example, the $V - H\alpha$ vs. $V - I$ color-color diagram for our field #1. We use the median $V - H\alpha$

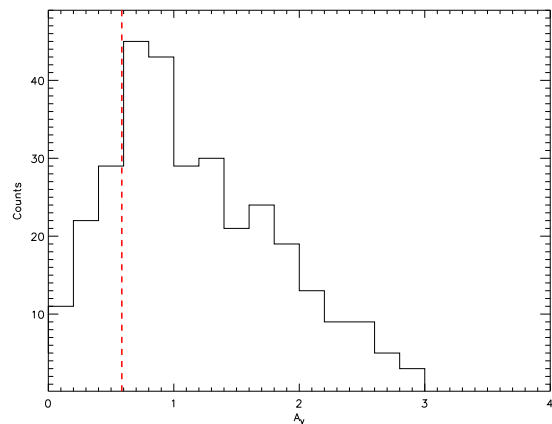


Figure 3. Example of A_V distribution for stars in a sub-image of our field #1. The dashed line indicates the 17th percentile of the distribution.

dereddened color of stars with small photometric errors in the V, I and H α bands ($\delta_3 = \sqrt{(\Delta V^2 + \Delta I^2 + \Delta H\alpha^2)}/3 < 0.15$) as a function of $V - I$ to define the reference template with respect to which the excess H α emission is sought (line in Figure 4). Since the contribution of the H α line to the V magnitude is completely negligible, the magnitude $\Delta H\alpha$ corresponding to the excess emission is simply:

$$\Delta H\alpha = (V - H\alpha)^{\text{obs}} - (V - H\alpha)^{\text{ref}} \quad (1)$$

where the superscript "obs" refers to the observations and "ref" to the reference template. We select a first sample of stars with excess H α emission by considering all those with $\delta_3 < 0.15$ and $V - H\alpha$ color above the reference template by 5 times their intrinsic photometric uncertainty ($\Delta H\alpha > 5 \times \sqrt{\Delta V^2 + \Delta H\alpha^2}$). Note that this threshold is somehow arbitrary; it affects the total number of selected PMS star candidates but not the typical \dot{M} of the selected PMS population, on which the conclusion of this paper are based (Sect. 6).

Then, we derive the equivalent width of the H α emission line ($EW_{H\alpha}$) from the measured $\Delta H\alpha$ as:

$$EW_{H\alpha} = RW \times [1 - 10^{-0.4 \times \Delta H\alpha}] \quad (2)$$

where RW is the rectangular width of the filter, which depends on the characteristics of the filter (see Table 4 in Paper I). We also

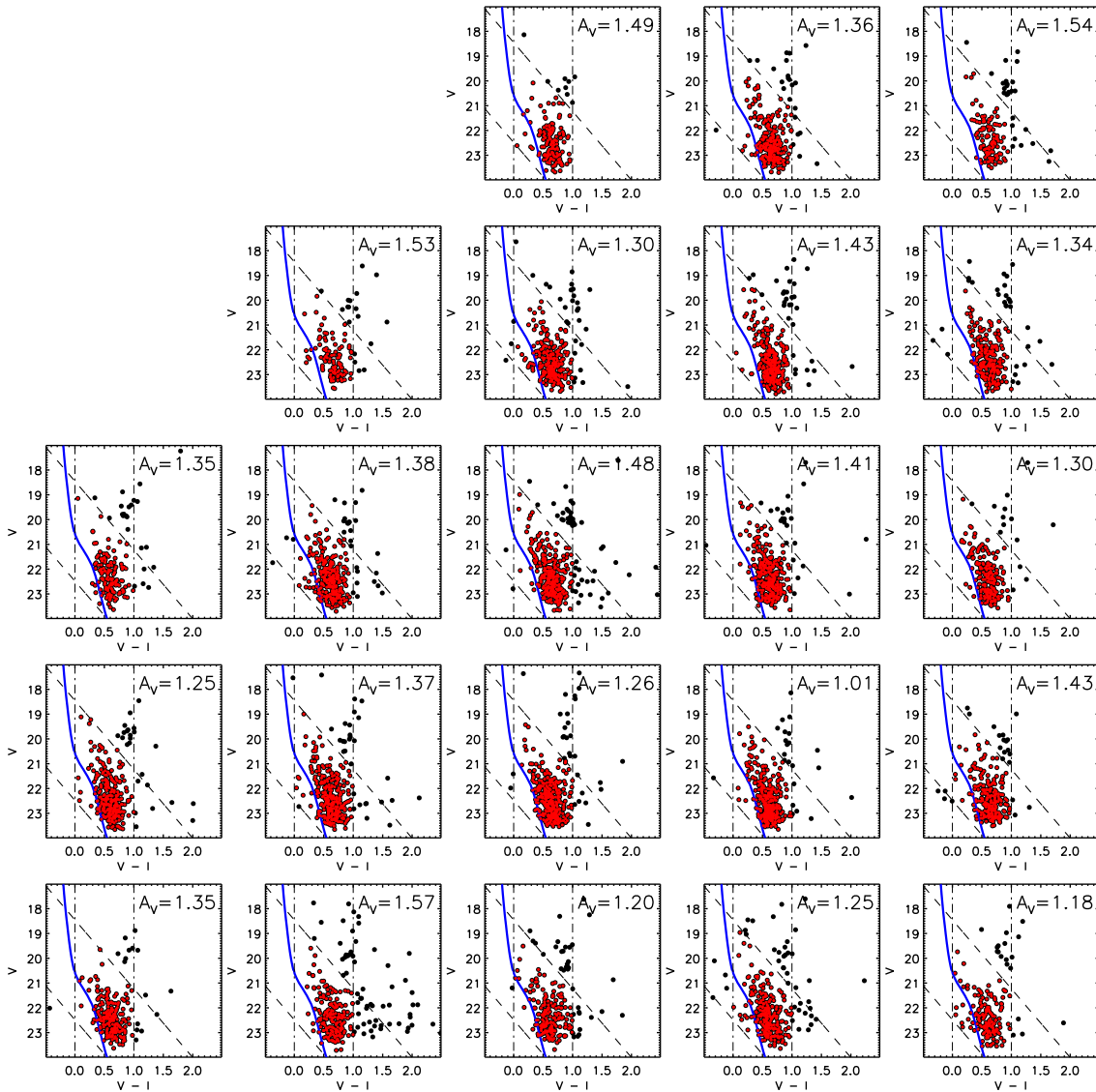


Figure 2. Example V vs. $V - I$ CMDs for one of our WFPC2 fields (field #1) divided into 22 $32'' \times 32''$ regions to study the spatial variation of the interstellar extinction over the observed field. The solid line is the ZAMS by Marigo et al. (2008). The dashed lines show the direction of the reddening vector and, together with the dashed dash-dotted lines, define the region of the CMD uncontaminated by stars in the red clump. The visual extinction assigned to each region is reported in the top-left of each panel.

derive the effective temperature (T_{eff}), radius (R_*) and luminosity (L_*) from the dereddened $V - I$ color and V magnitude. We adopt the distance of 51.4 kpc to the LMC (Panagia 1991; Panagia et al. 1991) and use the tabulation of HST/WFPC2 colors as a function of T_{eff} by Bessel et al. (1998).

Following the prescription of White & Basri (2003) and adopting the effective temperature vs. spectral type scale by Kenyon & Hartmann (1995), we finally consider as probable PMS stars those objects with (Figure 4, lower panel) $EW_{H\alpha} \geq 3 \text{ \AA}$ for stars earlier than K5 (i.e., $T_{eff} \geq 4350 \text{ K}$), $EW_{H\alpha} \geq 10 \text{ \AA}$ for K5-M3 stars ($3400 \leq T_{eff} < 4350 \text{ K}$) and $EW_{H\alpha} \geq 20 \text{ \AA}$ for M3-M6 stars ($3000 \leq T_{eff} < 3400 \text{ K}$). Our photometric limits are such that we do not detect LMC members later than M6 in any of the fields (see Sect. 2). We also reject stars with $V - I \leq 0$. These two criteria allow us to clean our sample from possible contaminants, i.e. older stars with chromospheric activity and Ae/Be stars, respectively.

Note that dKe and dMe stars with enhanced coronal

emission have $EW_{H\alpha}$ well below 20 \AA even during flares (Worden & Peterson 1976; Bopp & Schmitz 1978). Thus, the criterion by White & Basri (2003) allows us to safely remove dMe stars, while some the dKe might still be included in the PMS sample. We could use a more conservative threshold of $EW_{H\alpha} = 20 \text{ \AA}$ for both K and M type stars, as was done in Paper II. However, while avoiding contamination from magnetically active field stars, this threshold might cause the rejection of some of the weaker K0-K7 type accretors ($\dot{M} \lesssim 10^{-9} M_{\odot}/\text{yr}$; White & Basri 2003) and, hence, an over-estimation of the typical accretion rates of our PMS populations, in particular at ages older than $\sim 10 \text{ Myr}$. Thus, for K type stars we choose to adopt the more relaxed criterion of White & Basri (2003).

We identified 490 objects in our field #1, 325 in our field #2 and 242 in our field #3 with $H\alpha$ emission typical of accreting PMS stars. These numbers are of the same order of magnitude as the number of low-mass stars expected in each region on the basis of the number of OB stars (Sect. 8.4.2) and a typical IMF ($\alpha=2.35$;

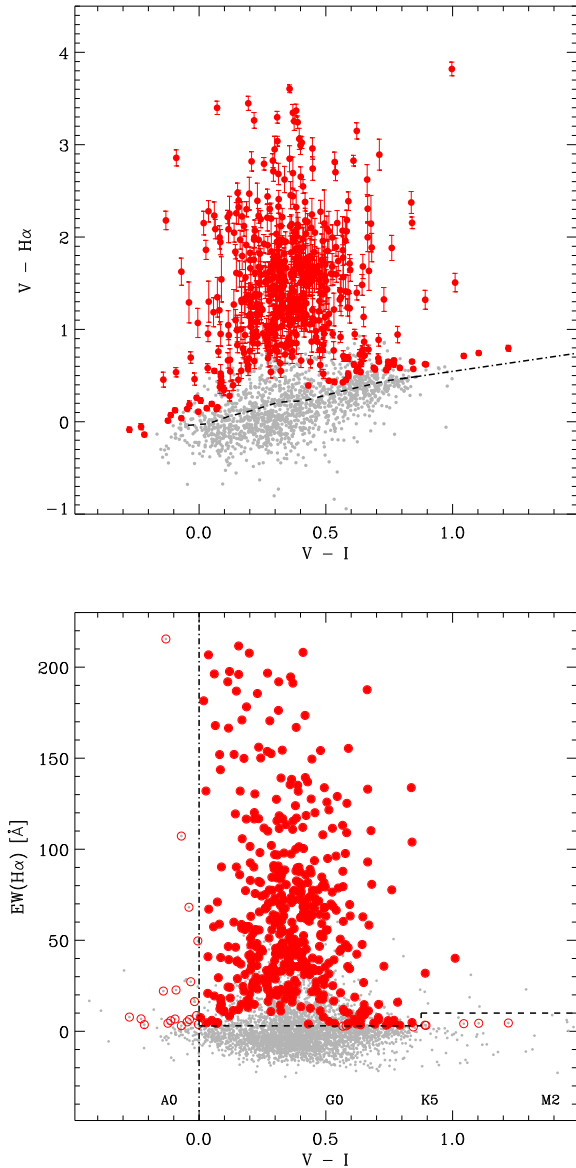


Figure 4. **Upper panel:** Example of $V - H\alpha$ vs. $V - I$ diagram of stars in one of our fields (field #1). The line is the reference template with respect to which the excess $H\alpha$ emission is sought. Objects with a $V - H\alpha$ excess are indicated as big dots with error bars. **Lower panel:** $H\alpha$ equivalent width as a function of $V - I$ for stars in field #1. Objects satisfying the White & Basri (2003) $EW_{H\alpha}$ criterion (dashed line) and redder than $V - I = 0$ (dot-dashed line) are considered PMS star candidates (big dots). The remaining objects (open circles) are older stars with chromospheric activity or Ae/Be stars.

Salpeter 1955), meaning that we are detecting a large fraction of accretors in those regions. This point is very important for the conclusions of this paper. As we will see in Sect. 6, the typical mass accretion rates in the LMC are higher than in the MW; because our samples are representative of the entire PMS population in the studied regions, we can be confident that this is not a selection effect.

3.3 Determination of mass and age

The mass (M_*) and age of each star are derived by comparing its L_* and T_{eff} with PMS evolutionary models. Specifically, we used

the Pisa database of PMS tracks and isochrones (Tognelli et al. 2011) for metallicity $Z=0.007$, as appropriate for the LMC, and followed the interpolation procedure developed by Romaniello (1998), which does not make assumptions on the properties of the population, such as the functional form of the IMF. On the basis of the measurement errors, this procedure provides the probability distribution for each individual star to have a given value of the mass and age (the method is conceptually identical to the one presented recently by Da Rio et al. (2010)).

Many caveats should be considered when dealing with masses and ages of PMS stars derived from evolutionary models. We will discuss them in detail in Sec. 7, because the uncertainty on these parameters, in particular on the isochronal age, could have a strong and unavoidable impact on our results. Here we stress that, although isochronal ages of individual objects are uncertain, given the presence of unresolved binaries and the stellar variability, ages of statistical samples are, in principle, reliable and the global age differences between regions are real (see, e.g., Mayne et al. 2007). This statistical approach is the one we use for the analysis illustrated in the next sections. Moreover, there are several arguments supporting the reliability of our age estimates:

(i) the median age estimated for our field #1 (13 Myr, Table 4), the closest one to supernova SN1987A, is roughly consistent with the age independently estimated for the progenitor of SN1987A and nearby stars (~ 13 Myr; Scuderi et al. 1996);

(ii) Figure 5 shows the HR diagram for the PMS populations of the four LMC regions under analysis. There is a clear difference between the distribution of PMS stars belonging to the youngest (#3, 6-8 Myr) and the oldest (SN1987A, 13 Myr) of our regions, with region #3 being clearly a few Myr younger than the SN1987A region. The age of regions #1 and #2 is intermediate between region #3 and the SN1987A region and their PMS population concentrate between 4 and 14 Myr, where the isochrones become very close to each other and it is hard to derive an age difference based only on the visual inspection of the HR diagram. However, as reported in Table 4, the median isochronal ages of region #1 and #2 differ by a few Myr and with respect to region #3 and the SN1987A region as well, and the difference is statistically significant.

(iii) Elmegreen (2000) showed that the age dispersion of a given stellar population depends on the size of the region. Taking into account the typical size of our region ($162'' \times 162''$, i.e. about 100 pc at the LMC distance), we would expect an age dispersion of a few to 10 Myr inside each region, which is consistent with our findings (Table 4).

3.4 Determination of the mass accretion rate

The mass accretion rate is derived from the free-fall equation as:

$$\log \dot{M} (M_{\odot}/yr) = -7.39 + \log \frac{L_{acc}}{L_{\odot}} + \log \frac{R_{*}}{R_{\odot}} - \log \frac{M_{*}}{M_{\odot}} \quad (3)$$

where L_{acc} is the energy released by the accretion process, directly proportional to the $H\alpha$ luminosity (Dahm 2008, and Paper I):

$$\log L_{acc} = (1.72 \pm 0.47) + \log L(H\alpha) \quad (4)$$

Once the color excess $\Delta H\alpha$ is determined, the $H\alpha$ emission line luminosity, $L(H\alpha)$, can be immediately obtained from the photometric zero point and absolute sensitivity of the instrumental set-up and from the distance to the sources (see Sect. 3.1 in Paper I).

The problems involved in measuring \dot{M} have been recently discussed by several authors (e.g., Herczeg & Hillenbrand 2008;

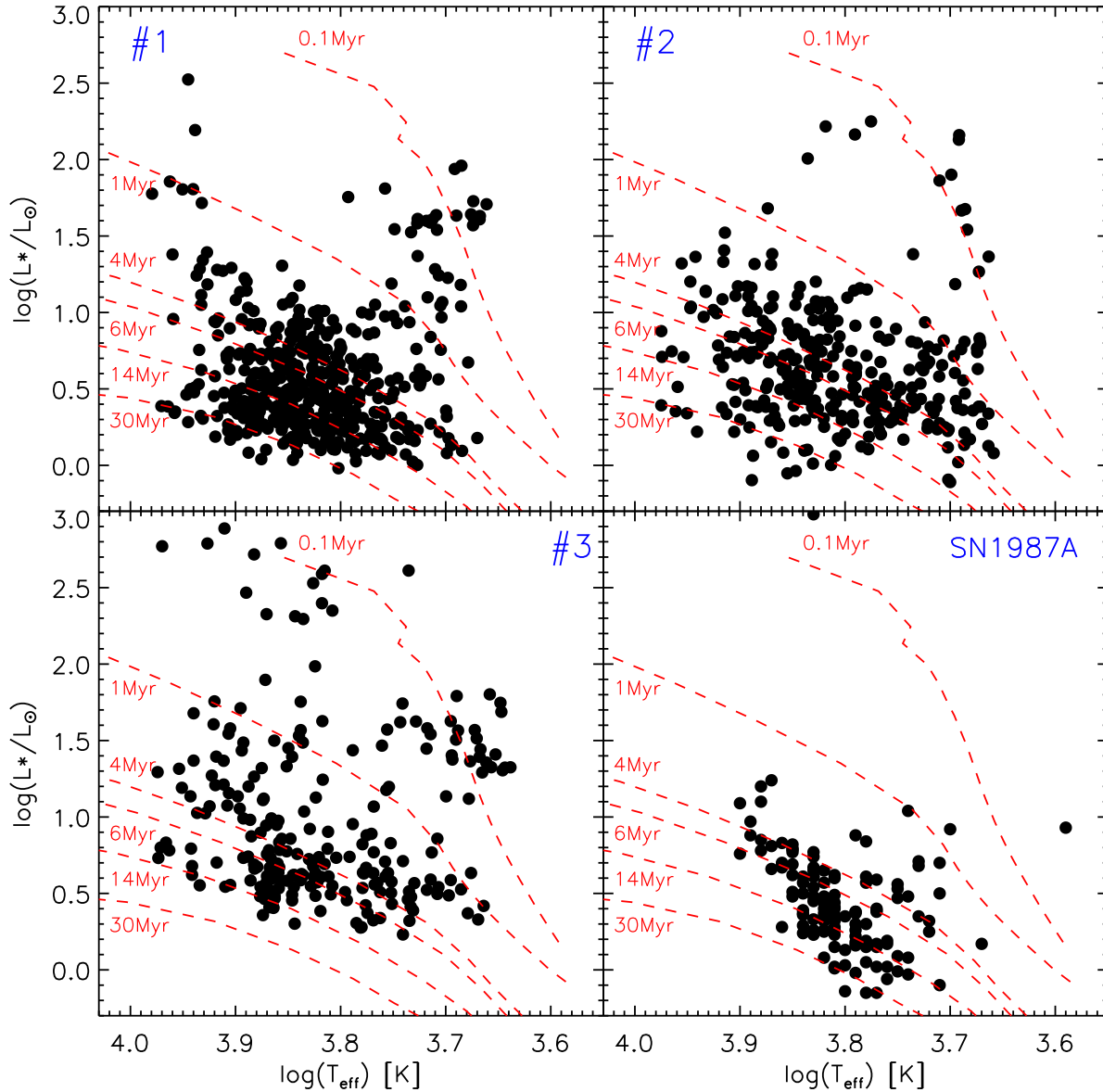


Figure 5. HR diagram for the PMS population in the four LMC regions under analysis. The dashed lines are the PMS isochrones by Tognelli et al. (2011) for the metallicity of the LMC. All objects shown here have $H\alpha$ excess emission and $H\alpha$ equivalent width above the levels discussed in Sect. 3.2.

Barentsen et al. 2011; Rigliaco et al. 2011) and measurements using different diagnostics might give different results by about an order of magnitude. The uncertainties of the $H\alpha$ diagnostics and the specific method adopted in this work have been fully addressed in Paper I. The typical error on $\log \dot{M}$ is of the order of 0.7-0.8 dex (see Table 3) and the main sources of this uncertainty are:

(i) The uncertainty on the L_{acc} vs. $L(H\alpha)$ calibration relation (Equation 4), which is based on near-infrared spectra of a dozen accreting members of the IC 348 cluster (see Figure 17 by Dahm 2008). Due to the poor statistics, the resulting uncertainty on L_{acc} is as high as a factor of 3. Moreover, the relation is mainly calibrated using stars with mass below $1 M_{\odot}$ and a handful of stars around $2 M_{\odot}$, while a gap in accreting stars is observed extending between 0.8 and $1.8 M_{\odot}$. Thus, this relation is more uncertain when applied to the mass regime considered in this paper (1-2 M_{\odot});

(ii) Systematic uncertainties due to i) discrepancies in the isochrones and evolutionary tracks, ii) reddening, iii) $H\alpha$ emission not due to the accretion process, and iv) the contribution of the nebular continuum to the colors of the stars. In Paper I we discussed in detail these four contributions and concluded that: i) systematic uncertainties of the order of 20% are to be expected for the mass due to differences between evolutionary models; ii) for an average LMC star-forming region, omitting the extinction correction would result in a 10% overestimate of \dot{M} . This error is smaller in our case, because our photometric catalogs are dereddened taking into account the effect of patchy absorption (Sect. 3.1); iii) possible sources of $H\alpha$ emission other than accretion are chromospheric activity, whose contribution is 2 orders of magnitude less than what we measure, $H\alpha$ emission along the line of sight arising in knots of ionized H (e.g., very compact HII), which we removed by a vi-

sual inspection of all objects with excess $H\alpha$ emission, and gaseous regions around the object ionized by an external source (e.g., hot ionizing stars), which, according to the calculation presented in Paper I (Table 1), is negligible in our case because there are no OB stars in the close vicinity ($<5''$) of our PMS star candidates (see Sect. 8.4.2). We can, therefore, conclude that in our fields the contribution of $H\alpha$ emission generated by sources other than the accretion is negligible; iv) if present, nebular continuum will add to the intrinsic continuum of the star, thereby affecting the observed broad-bands colors of the source. As shown in Paper I (Table 2), for the typical spectral range of our candidates (G-K), the effects of the nebular continuum on the $V - I$ color of PMS stars remains insignificant even for the PMS objects with the highest $EW_{H\alpha}$;

(iii) Other possible systematic errors on the mass and age estimates due to inaccuracies in the models' input physics, which we will discuss in Sect. 7;

(iv) As for the statistical uncertainty on other quantities in Equation 4 and 3, they are as follows. With our selection criteria, the typical uncertainty on $L(H\alpha)$ is 15% and is dominated by random errors. The uncertainty on R_* is typically 7%, including a 5% systematic uncertainty on the distance modulus. As for the mass M_* , since it is determined by comparing the location of the star in the HR diagram with evolutionary tracks, both systematic and statistical uncertainties are important. The uncertainty on the temperature is mostly statistical and is about 3%, while that on the luminosity is 7%, comprising both random errors (1% uncertainty on the bolometric correction and 3% on the photometry) and systematic effects (5% uncertainty on the distance modulus). When we interpolate through the PMS evolutionary tracks to estimate the mass, the uncertainties on T_{eff} and L_* imply an error of 7% on M_* . In summary, the combined statistical uncertainty on \dot{M} is 17%.

4 THE NEW SAMPLE OF ACCRETING PMS STAR CANDIDATES IN THE LMC

We have determined the mass accretion rates for 490 PMS star candidates in our field #1, 325 in our field #2 and 242 in our field #3. Adding the 106 PMS stars in the field around supernova SN1987A characterized in Paper I, we end up with a sample of about 1000 PMS star candidates in the LMC with mass between 1 and 5 M_\odot and age between ~ 1 and 30 Myr. Our sample represents the largest \dot{M} dataset for low-metallicity stars presented so far. The majority of our PMS stars ($\sim 90\%$) have masses below 2 M_\odot , i.e. in the T Tauri star range. The remaining $\sim 10\%$ are Herbig Ae/Be stars; at the typical age of our regions (Table 4), many of them could already approach or be on the main sequence. Moreover, they cannot be considered simply as massive counterparts of T Tauri stars because they are characterized by different properties (strong winds, small magnetic fields, etc.; Herbig 1960; Waters & Waelkens 1998). Thus, the $H\alpha$ vs. \dot{M} calibration used for T Tauri stars (Equation 4) might be inappropriate for Herbig Ae/Be stars and, hence, the \dot{M} derived for these objects might be inaccurate. This does not affect the results presented in this paper because, as explained in Sect. 2, we limit our analysis to the range 1-2 M_\odot .

HST/WFPC2 photometry, stellar parameters and mass accretion rates for this sample are available, only in electronic form, in Table 2 and 3, respectively. In Table 4 we summarize the number of PMS stars selected in each field and their median mass, age and mass accretion rate. Using this large sample of PMS stars with \dot{M} measured in a homogeneous way, we now investigate the depen-

dency of \dot{M} on stellar mass, age and metallicity, in relation with the proposed mechanisms of disk dispersal.

4.1 On the completeness of our accreting PMS star sample

In Sect. 2 we estimated that our observations for field #1, #2 and #3 are photometrically complete in all the filters in the mass range 1-2 M_\odot for 1 to 14 Myr old objects at the distance of the LMC and, hence, in this section we limit our analysis to this mass range. However, the mass accretion rate of PMS stars depends on the stellar mass (Muzerolle et al. 2005; Natta et al. 2006; Sicilia-Aguilar et al. 2006) and decreases with time (Muzerolle et al. 2000; Sicilia-Aguilar et al. 2005, 2006, 2010; Fedele et al. 2010). Thus, our limit for the measurement of \dot{M} varies within the considered mass and age range.

Figure 6 shows the \dot{M} of PMS star candidates in our sample as a function of mass (upper panel) and age (lower panel). In each panel, the dashed line displays our photometric limit for the detection of excess $H\alpha$ emission and, hence, for the measurement of \dot{M} . In order to translate the detection limit in $H\alpha$ luminosity into the detection limit in \dot{M} as a function of stellar mass, we considered the lowest $H\alpha$ luminosity measured for our PMS stars and used Equ. 3 and 4. We assumed the median age of all PMS star candidates in our sample (10 Myrs) and calculated the corresponding stellar radii for different stellar masses using the 10 Myr isochrone for the metallicity of the LMC. Analogously, we translated the detection limit in $H\alpha$ luminosity into the detection limit in \dot{M} as a function of stellar age by using Equ. 3 and 4 and assuming the lowest $H\alpha$ luminosity measured for our PMS star candidates and their median mass (1.4 M_\odot); we then calculated the corresponding stellar radii from the 1.4 M_\odot evolutionary track for the metallicity of the LMC.

Figure 6 and the limiting magnitudes in Table 1 show that our photometric limits allow us to detect only the brightest and, hence, youngest accreting late K-type stars at the distance of the LMC, while they are sufficient to detect early K or G-type accreting stars ($M_* \gtrsim 1.3M_\odot$) of any age up to the main sequence. In particular, the lower panel of Figure 6 shows that our PMS star candidates define a bulge of points at ages around 10 Myrs and this bulge is very close to the photometric limit; this implies that we might have missed part of the PMS objects with very low accretion rates at ages around 10 Myr. At younger ages, the mass accretion process of PMS stars is enhanced and the $H\alpha$ luminosity increases; if more accreting PMS stars younger than 10 Myr were present, we would have them. In summary, our accreting PMS star candidate sample in the LMC is complete in the spanned age range for $M_* \gtrsim 1.3M_\odot$, while we might have missed part of the oldest lower-mass accreting stars.

We now quantify this incompleteness effect by using the dataset presented in Paper I as a reference. Indeed, one of the main objectives of this work is to compare the accreting properties of PMS stars in our LMC fields with the pioneer study presented in Paper I, where we found that the \dot{M} of PMS stars in the region around supernova SN1987A are systematically higher than their Galactic counterparts (Sect. 6). To make sure that this comparison is performed in a homogeneous way, we derived a correction to be applied to the typical \dot{M} measured in our LMC fields to match the completeness of the Paper I dataset. We proceeded as follows.

Since the photometric catalog for the SN1987A region (Paper I) is much deeper than our catalogs, it can be considered as a reference catalog with 100% completeness for the measurement of \dot{M} in the considered mass range (1-2 M_\odot). We considered the $H\alpha$ luminosity ($L(H\alpha)$) distribution of PMS stars in the field around

Table 2. Astrometry and observed photometry of the PMS star candidates in the LMC.

Field	ID	RAJ2000 (hh:mm:ss)	DECJ2000 (dd:mm:ss)	F606W	F656N	F814W
#1	1	5:34:47.62	-69:14:37.89	22.435±0.028	20.463±0.109	21.957±0.028
#1	2	5:34:44.36	-69:15:13.14	21.028±0.012	19.631±0.051	20.220±0.010
#1	3	5:34:43.90	-69:15:17.41	21.549±0.015	20.408±0.092	21.061±0.015
#1	4	5:34:45.31	-69:15: 1.14	19.870±0.008	18.990±0.027	19.142±0.007
#1	5	5:34:47.21	-69:14:41.45	19.789±0.008	18.839±0.024	18.984±0.006
#2	1	5:35:41.65	-69: 9:10.82	20.484±0.002	18.439±0.017	19.527±0.002
#2	2	5:35:41.40	-69: 9: 8.94	23.139±0.035	20.382±0.092	22.338±0.038
#2	3	5:35:41.55	-69: 9: 8.70	22.368±0.016	20.311±0.103	21.878±0.018
#2	4	5:35:41.69	-69: 9: 8.25	22.095±0.009	20.610±0.111	21.569±0.012
#2	5	5:35:41.93	-69: 9: 8.08	21.438±0.005	19.892±0.060	20.738±0.006
#3-Pop.1	1	5:39:32.88	-69: 9:34.32	20.324±0.011	16.878±0.013	19.452±0.009
#3-Pop.1	2	5:39:36.03	-69: 9: 8.81	20.434±0.011	19.061±0.060	19.432±0.010
#3-Pop.1	3	5:39:32.47	-69: 9:40.29	21.993±0.036	18.877±0.067	21.842±0.034
#3-Pop.1	4	5:39:32.94	-69: 9:36.18	20.604±0.012	19.311±0.082	20.331±0.014
#3-Pop.1	5	5:39:35.28	-69: 9:16.37	21.993±0.024	20.400±0.134	21.354±0.021

Table 3. Stellar parameters, $H\alpha$ equivalent width and accretion rate of the PMS star candidates in the LMC.

Field	ID	$\log T_{eff}$ (K)	$\log L_{\star}/L_{\odot}$	Mass (M_{\odot})	Age (Myr)	$EW_{H\alpha}$ (\AA)	$\log \dot{M}_{acc}$ (M_{\odot}/yr)
#1	1	3.86±0.02	0.55±0.09	1.3	17.7	67± 9	-7.4±0.8
#1	2	3.72±0.01	1.10±0.04	2.3	0.6	18± 2	-7.1±0.8
#1	3	3.86±0.01	0.90±0.05	1.5	9.2	16± 3	-7.6±0.8
#1	4	3.75±0.00	1.54±0.03	3.2	0.7	4± 0	-7.2±0.8
#1	5	3.73±0.00	1.61±0.03	3.5	0.3	3± 0	-7.2±0.8
#2	1	3.66±0.00	1.37±0.02	1.2	0.0	58± 1	-5.8±0.7
#2	2	3.71±0.02	0.24±0.12	1.3	5.9	158±16	-7.2±0.8
#2	3	3.84±0.01	0.53±0.06	1.3	16.4	73± 9	-7.4±0.8
#2	4	3.83±0.01	0.63±0.04	1.3	12.0	31± 6	-7.6±0.8
#2	5	3.75±0.00	0.89±0.03	2.0	2.7	32± 3	-7.2±0.7
#3-Pop.1	1	3.68±0.00	1.36±0.04	1.4	0.1	292± 5	-5.3±0.7
#3-Pop.1	2	3.67±0.00	1.44±0.04	1.4	0.0	17± 2	-6.4±0.8
#3-Pop.1	3	3.97±0.04	0.73±0.19	1.6	8.5	245±19	-7.0±0.8
#3-Pop.1	4	3.91±0.01	1.21±0.04	1.8	6.2	21± 3	-7.2±0.8
#3-Pop.1	5	3.80±0.01	0.73±0.08	1.4	8.5	29± 7	-7.4±0.8

SN1987A and derived its peak by performing a Gaussian fit (Figure 7). This peak ($L(H\alpha)_{Ref}$) represents the limit of this dataset for the detection of $H\alpha$ excess emission and, hence, for the measure of \dot{M} .

In Figure 7 we compare the $L(H\alpha)$ distribution of the SN1987A PMS population with the analogous distributions for our region #1. This region is very close to SN1987A, has the same age (Table 4) and is part of the same star-forming complex. Thus, the difference between the peak of this distribution and $L(H\alpha)_{Ref}$ represent the $L(H\alpha)$ correction to be applied to field #1 to match the completeness of the SN1987A dataset. The $L(H\alpha)$ correction has been translated into \dot{M} correction by using Equ. 3 and 4, assuming the median mass and age of the PMS population in region # as reported in Table 4 and using the relative evolutionary model for the metallicity of the LMC to calculate the corresponding stellar radius.

The $H\alpha$ observations of fields #2 and #3 have roughly the

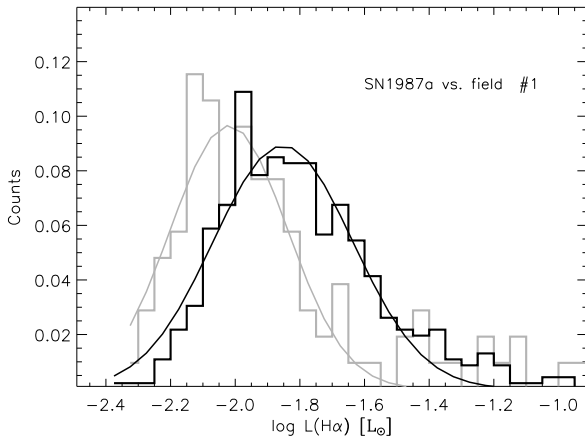
same photometric depth as field #1 (Table 1) and, hence, we assume the same \dot{M} correction. The median \dot{M} of the PMS star candidates selected in each field corrected for completeness are reported in Table 4.

5 ON THE MASS DEPENDENCY OF THE MASS ACCRETION RATE IN THE LMC

The mass accretion rate of galactic PMS stars appears to be roughly proportional to the second power of the stellar mass over a wide range (0.3-3 M_{\odot} ; Natta et al. 2004; Mohanty et al. 2005; Natta et al. 2006; Muzerolle et al. 2005; Sicilia-Aguilar et al. 2006), with a large spread of two orders of magnitude at least for any interval of M_{\star} . Recent observations also show that this power law might even be steeper ($\dot{M} \propto M_{\star}^{3.1}$) in the very low-mass and sub-solar mass domain ($M_{\star} \lesssim 0.4M_{\odot}$), while flatten-

Table 4. Number of PMS stars selected in each field and their median mass, age and mass accretion rate. For each parameter the range spanned by each PMS population and the standard deviation of the distributions (σ) are also given.

Field	N. of PMS stars	Median Mass (M_{\odot})	Median Age (Myr)	Median $\log \dot{M}^{\dagger}$ (M_{\odot}/yr)	Corrected $\log \dot{M}^{\ddagger}$ (M_{\odot}/yr)
#1	490	1.3 range [1: 5] $\sigma=0.5$	13 range [1: 30] $\sigma=6$	-7.5 range [-8.1: -6.3] $\sigma=0.3$	-7.6
#2	325	1.4 range [1: 5] $\sigma=0.5$	9 range [1: 30] $\sigma=6$	-7.3 range [-7.7: -5.3] $\sigma=0.5$	-7.4
#3 - Pop. 1	96	1.4 range [1: 4] $\sigma=0.4$	8 range [1: 25] $\sigma=6$	-7.1 range [-7.5: -5.1] $\sigma=0.5$	-7.2
#3 - Pop. 2	146	1.5 range [1: 5] $\sigma=1$	6 range [1:30] $\sigma=6$	-7.1 range [-7.9: -5.3] $\sigma=0.5$	-7.2
SN1987A ^a	104	1.3 range [1: 2.2] $\sigma=0.2$	14 range [1: 30] $\sigma=6$	-7.59 range [-8.0: -6.4] $\sigma=0.3$	–

^aFrom Paper I.[†]Median mass accretion rate in the mass range 1-2 M_{\odot} .[‡]Median mass accretion rate in the mass range 1-2 M_{\odot} corrected for completeness effects (Sect. 4.1).**Figure 7.** Comparison between the $H\alpha$ luminosity distribution of the PMS population in the region around SN1987A (gray histogram, from Paper I) and the distribution for our fields #1 (black histogram). The curves show the Gaussian fit to the data.

ing ($\dot{M} \propto M_{\star}^2$ or even flatter) when only the $M_{\star} \gtrsim 0.8M_{\odot}$ domain is considered (Fang et al. 2009; Sicilia-Aguilar et al. 2010). This seems to support the idea that the accretion and disk evolution process might present important differences for low and high-mass stars (Hartmann et al. 2006).

The large spread observed in the \dot{M} vs. M_{\star} dependency partly arises from the uncertainty in the determination of \dot{M} , which can be as high as one order of magnitude. However, this relation still contains an intrinsic scatter due to the age dependency of \dot{M} , individual disk properties and the variability of the mass accretion process, as discussed in Sect. 1. Indeed, mass accretion rates for younger stars tend to be higher, as expected from the viscous disk

evolutionary models (Hartmann et al. 1998). The \dot{M} versus age dependency appears to be very steep, with \dot{M} decreasing by more than three order of magnitude within the first 10 Myr of the stellar life (see Figure 2 by Sicilia-Aguilar et al. 2010). This effect is likely to increase the spread in \dot{M} for any interval of M_{\star} , because the PMS populations in young clusters and star forming regions in the MW generally present an age spread of a few Myr (Jeffries 2011), and objects progressively younger are expected to form parallel trends in the \dot{M} vs. M_{\star} relation with increasing offset in \dot{M} (see, e.g., Sicilia-Aguilar et al. 2006, 2010).

We now use our sample of PMS stars to investigate the \dot{M} versus M_{\star} correlation in the LMC. Although our sample spans a wide range of stellar masses (see Table 4), 90% of the PMS stars have masses between 1 and 2 M_{\odot} and, thus, we limit our analysis to this range, in order to obtain statistically robust results. We find that best fit to the \dot{M} versus M_{\star} dependency in the LMC is a linear correlation (Figure 6, upper panel). In order to investigate quantitatively this dependency, disentangling the dependency on age, we performed a double linear regression fit, setting M_{\star} and age as independent variables and \dot{M} as dependent variable. In a logarithmic scale, the functional form of this regression is as follows:

$$\log \frac{\dot{M}}{M_{\odot}\text{yr}^{-1}} = a \cdot \log \text{Age}(\text{Myr}) + b \cdot \log \frac{M_{\star}}{M_{\odot}} + c \quad (5)$$

where c is the offset and b and a the coefficients enclosing the mass and age dependency, respectively. In this section, we focus our attention of the mass dependency of \dot{M} enclosed in the b parameter. The age dependency and the relative a parameter will be discussed in the Sect. 6.

Considering all the PMS stars in the range 1-2 M_{\odot} , we find that the \dot{M} of PMS stars in the LMC increases almost linearly with stellar mass ($b = 0.82 \pm 0.16$, i.e. $\dot{M} \propto M_{\star}$). The solid line in Figure 6 (upper panel) displays the results of our linear regression fit; the dashed line displays our photometric limit for the detection of excess H_{α} emission and, hence, for the measurement of \dot{M} (Sect. 4.1).

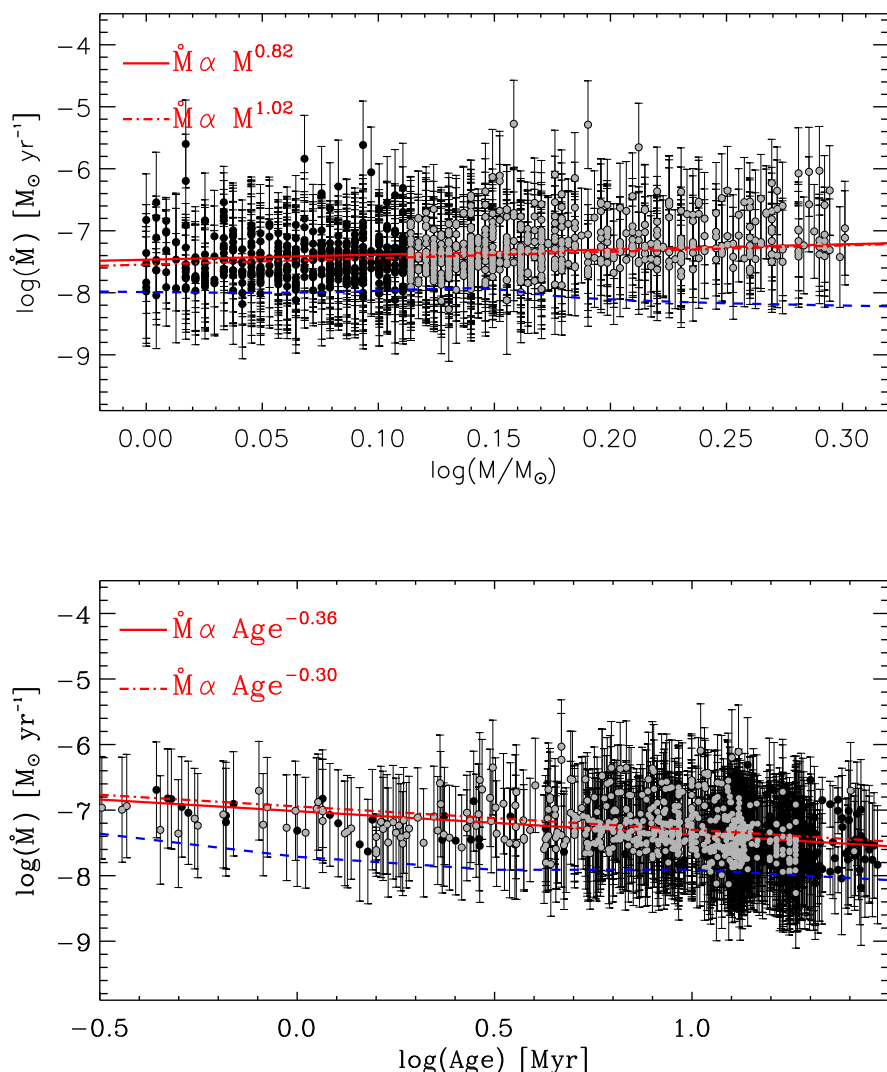


Figure 6. Mass accretion rate as a function of the stellar mass (upper panel) and age (lower panel) for PMS star candidates in the LMC with masses in the range $1\text{-}2 M_{\odot}$. In both panels, the solid line displays the result of the double linear regression fit to the points obtained by setting M_{\star} and age as independent variables and \dot{M} as dependent variable, while the dashed line represents our photometric limit for the measurement of \dot{M} (Sect. 5 and 6). The gray dots are the data points in the $M_{\star} \geq 1.3 M_{\odot}$ mass range, where our PMS star candidate sample is photometrically complete. The dot-dashed line displays the result of the double linear regression fit of this sub-set of data.

In order to avoid the mass regime where our survey is not complete, we recomputed the coefficients in Equ. 5 limiting the regression fit to the $M_{\star} \geq 1.3 M_{\odot}$ range (grey points and dot-dashed line in Figure 6). In this case, we obtain $b = 1.02 \pm 0.31$, confirming that the \dot{M} vs. M_{\star} dependency is roughly linear.

We conclude that in the approximate range $1\text{-}2 M_{\odot}$, the \dot{M} of PMS stars in the LMC increases with the stellar mass as $\dot{M} \propto M_{\star}^b$ where $b \approx 1$, in agreement with the value ($b = 0.9 \pm 0.1$) found for the PMS population of NGC 346 in the SMC (Paper II). Taking into account the uncertainty on the b -parameter, this dependency is slightly flatter than the second power law reported in the same mass range for samples of PMS stars in the Galaxy. Using data from the IPHAS survey of PMS stars in the galactic HII region IC 1396, Barentsen et al. (2011) also found a slope between 1.2 and 1.3 for

the \dot{M} vs. M_{\star} dependency, i.e. less steep than claimed in previous literature.

6 \dot{M} EVOLUTION AND METALLICITY DEPENDENCY

The data collected so far for galactic PMS stars indicate that \dot{M} is a decreasing function of stellar age (Muzerolle et al. 2000; Sicilia-Aguilar et al. 2005, 2006, 2010; Fedele et al. 2010), roughly in line with the expected evolution of viscous discs (Hartmann et al. 1998), although the spread of the data is very large (Sect. 1). More precisely, Fedele et al. (2010) estimated a mass accretion timescale (τ_{acc}) of 2.3 Myr for galactic PMS stars in the spectral type range K0-M5. Moreover, in the pioneering study of the mass accretion process in the MCc presented in Paper I and Paper II, we found that, in the field around supernova SN1987A in the LMC and in

NGC 346 in the Small Magellanic Cloud (SMC), the \dot{M} of PMS stars are systematically higher than their galactic counterparts.

Because of the very large uncertainties affecting age and \dot{M} determinations, one must be very careful when doing such a comparison for individual young stars. In particular, isochronal age estimates for PMS stars in the MCs are more uncertain than ages of galactic PMS stars, that can be confirmed by other methods (turnoff of the main sequence, dynamical evolution of the gas, etc.), and star forming regions in the MW are usually smaller and, hence, present smaller age dispersion (Elmegreen 2000). However, age differences based on statistical samples are more reliable.

In this section, we investigate the \dot{M} evolution in the MCs compared to the MW and verify the result by (De Marchi et al. 2010, 2011a). We dispose of an enlarged sample of PMS stars in the LMC with \dot{M} measured in a homogeneous way and, hence, we adopt a robust statistical approach which is expected to reduce as much as possible the effect of uncertainties on age/ \dot{M} . However, there are unavoidable caveats that might affect our results and we will discuss them in detail in Sect. 7.

Figure 6 (lower panel) gives a first hint on the time evolution of \dot{M} in the LMC, which, as expected, decreases with age. In order to investigate quantitatively the \dot{M} in the LMC we used at first the linear regression fit already describe in Sect. 5 (Equation 5) and shown by the solid line in Figure 6 (lower panel). We obtain $a \approx 1/3$, both when considering all the mass range 1-2 M_{\odot} and when limiting the fit to the $M_{\star} \gtrsim 1.3M_{\odot}$ regime to avoid incompleteness effects. This would imply that the \dot{M} of PMS stars in the LMC decreases with age significantly more slowly than observed for Galactic PMS stars of the same mass ($a \approx 1.2$; Sicilia-Aguilar et al. 2010), where the \dot{M} evolution is marginally consistent, though still slower, than the prediction of the viscous disk evolution model ($a=1.4-2.8$; Hartmann et al. 1998). This comparison is based on age/ \dot{M} estimates for single stars and there are at least two main problems affecting its outcome:

(i) In Sect. 3.3 we have already pointed out that isochronal ages of individual objects are uncertain, especially below a few Myr, and only ages and age differences of statistical samples should be trusted.

(ii) Sicilia-Aguilar et al. (2010) already pointed out that the difference between the observed \dot{M} evolution and prediction of the viscous disk model might be attributable to the fact that solar-type objects present a variety in the viscosity parameter radial exponent (Isella et al. 2009) and long-surviving disks may be biased toward certain radial viscosity laws.

A more robust approach to study the evolution of \dot{M} in the MCs in comparison to our MW consists of deriving the median age and \dot{M} of a sample of star forming regions in both galaxies spanning a suitable age range. We have collected from the literature 17 Galactic star-forming regions and clusters with ages between 1 and 30 Myr whose stellar population is well characterized in terms of \dot{M} . We considered only Galactic PMS stars with mass in the range 1-2 M_{\odot} , i.e. the range we are studying in the LMC. This sample consists of ~ 170 objects; their typical age and median \dot{M} , together with the number statistics per age bin and the reference papers, are reported in Table 5.

In Figure 8 we plot the median \dot{M} as a function of the median age for each one of these 18 Galactic PMS populations, for the LMC populations studied in this paper and for NGC 346 in the SMC (De Marchi et al. 2011a, hereafter Paper II). Note that NGC 346 displays two different stellar populations with median ages of ~ 1 (NGC 346-young) and ~ 20 Myr (NGC 346-old), re-

spectively, and our field #3 in the LMC also presents two spatially separated PMS populations (#3-Pop. 1 and #3-Pop. 2) with slightly different median ages (6 and 7 Myr, see Sect. 8.4). Thus, we dispose of 7 regions in the MCs with ages between 1 and 20 Myr (Table 4). The errors bars in Figure 8 for the MCs points are computed as the typical standard deviation of the \dot{M} and age distribution of each population plus the intrinsic uncertainty on these parameters. For the Galactic regions we adopt the typical error on \dot{M} and age estimated by Sicilia-Aguilar et al. (2006).

The analysis of Figure 8 reveals that below 3 Myr the only information we have at the moment in the MCs comes from NGC 346 in the SMC. Moreover, in this age range the number statistics of Galactic PMS stars with mass between 1 and 2 M_{\odot} and measured \dot{M} is very poor (i.e. only $\sim 10\%$ of the Galactic sample). As discussed in Sect. 7, below 3 Myr age determination becomes critical. Thus, we focus on the age range >3 Myrs and defer the analysis of the very young regime (1-2 Myr) to a future paper based on improved number statistic of 1-3 Myr old PMS stars in the core of the 30 Doradus starburst cluster (De Marchi et al. 2011b).

After the first 3 Myr, despite the large uncertainties, the average \dot{M} of PMS stars in the MCs is systematically higher than that of Galactic PMS stars of the the same age, confirming the results by Paper I. Note that the pentagrams in Figure 8 display the median \dot{M} for the two PMS populations in the Orion Nebular Cluster (ONC-young and ONC-old, see Table 5) and the diamond corresponds to Trumpler 37 (Tr 37), for which mass accretion rates are photometrically derived by Panagia et al. (2011, in preparation) and Barentsen et al. (2011), respectively, using the same method adopted in this paper. These three points follow very well the Galactic trend. In particular, the median \dot{M} measured by Barentsen et al. (2011) for the PMS population in Tr 37 perfectly agrees with the median \dot{M} measured by Sicilia-Aguilar et al. (2006, 2010) for the same population on the basis of U-band excess emission and high resolution spectroscopy, which provides accurate spectral type and reddening estimate. This demonstrates that the difference in the typical \dot{M} between the MCs and the MW is not due to systematic uncertainties of the photometric method we use to measure \dot{M} .

If we perform a linear fit to these averaged data for ages above 3 Myrs, we find that in the MCs \dot{M} decreases with time as $\dot{M} \propto t^{-a}$ with $a = 1.5 \pm 0.2$, confirming the average trend in the MW ($a = 2.6 \pm 1.0$) and in agreement with the prediction of viscous disk evolution models ($a=1.4-2.8$; Hartmann et al. 1998).

Being the metallicity of the MCs considerably lower than the MW, Figure 8 suggests a tantalizing metallicity dependency of the mass accretion process, specifically that \dot{M} appears to be inversely proportional to stellar metallicity. Under this hypothesis, we should observe some difference in \dot{M} even between the two MCs, because their metal content is different ($Z=0.007$ for LMC and $Z=0.002$ for SMC; Maeder et al. 1999) and the difference is comparable with the difference between the LMC and the MW ($Z \approx 0.018$). We do not observe such a difference when considering the mean \dot{M} values, as we did in our Figure 8. However, Paper II (focused on the the SMC cluster NGC 346 and based on individual age and \dot{M} measurements) indicates that there is a difference between the two MCs and \dot{M} in the SMC seems to be slightly higher than in the LMC. This would fit the idea of \dot{M} being inversely proportional to the metallicity.

These results suggest that the mass accretion process in the MCs might be different from the typical mechanism observed in Galactic PMS stars in two main aspects, which are discussed in the following sub-sections. In Sect. 7 we will further discuss these

Table 5. Median \dot{M} and number statistics per age bin for galactic PMS populations in the mass range 1-2 M_{\odot} .

Galactic region	Typical Age (Myr)	Median $\log \dot{M}$ (M_{\odot}/yr)	Number of members with $1 \leq M/M_{\odot} \leq 2$	Ref.
ρ -Ophiuchus [†] (ρ -Oph)	0.5	-7.95	4	Natta et al. (2006)
Orion Nebula Cluster (ONC-young)	3	-7.60	9	Panagia et al. 2011 (in preparation)
Orion Nebula Cluster (ONC-old) [‡]	12	-9.00	9	
IC 348 Lupus III (LupIII) σ -Orionis (σ -Ori) Taurus (Tau)	2-3	-7.81	9	Dahm (2008) Herczeg & Hillenbrand (2008) Rigliaco et al. (2011) Calvet et al. (2004)
Trumpler 37 (Tr37) Chamaeleon II (ChaII)	4	-9.49	88	Sicilia-Aguilar et al. (2006, 2010); Barentsen et al. (2011) Spezzi et al. (2008)
η -Chamaeleontis (η -Cha) Orion OB 1c Association (Ori-OB1c) λ -Orionis (λ -Ori)	5-7	-8.98	7	Jayawardhana et al. (2006) Calvet et al. (2004) Calvet et al. (2004)
Hydrae (Hya)	8-10	-10.52	4	Pinzón et al. (2007); Jayawardhana et al. (2006)
β -Pictoris (β -Pic) NGC 7160	12	-10.26	5	Pinzón et al. (2007); Sicilia-Aguilar et al. (2010) Sicilia-Aguilar et al. (2010)
Lower Centaurus Crux (LCC) Upper Centaurus Lupus (UCL)	16	-8.32	40	Pinzón et al. (2007) Pinzón et al. (2007)
Tucana-Horologium (Tuc-Hor)	30	-11.03	8	Pinzón et al. (2007); Jayawardhana et al. (2006)

[†]Note that, while the age of ρ -Oph is often listed as ~ 0.5 Myr, Wilking et al. (2008) state that the the well characterized, optically visible PMS stars might be as old as 2-5 Myr. Thus, in Figure 8 we indicate with an arrow the possible age range spanned by ρ -Oph members.

[‡]For the ONC-old population we report the minimum age estimated by Panagia et al. (2011, in preparation).

results considering the many caveats of current PMS evolutionary models, which might affect age estimates both in the MCs and in our MW and hence, our results. We will also review the main mechanisms of disk dispersal (Sect. 8) in order to understand whether the lower metallicity of the MCs with respect to the MW plays in favor of a typically higher \dot{M} .

6.1 Disk lifetime

For PMS stars in the MW most signs of accretion disappear after ~ 10 Myr. This, together with the observation that the fraction of stars with near-IR excess, which originate from the hot dust in the inner disk, decreases at a constant rate (Haisch et al. 2001; Sicilia-Aguilar et al. 2006), yields an overall disk lifetime of about 5-6 Myrs. However, a few cases of strong accretors at older ages have been reported in the literature. Sicilia-Aguilar et al. (2005) notice the presence of several Galactic G-type stars, with an apparent age older than ~ 10 Myr, showing higher accretion rates outside the typical trend of Galactic PMS stars (see their Figure 12). However, they warn that their age estimates might be significantly affected by the uncertainties in the birth line for G-type stars (see Sect. 7). More recently, Baume et al. (2011) also found a handful of stars with $H\alpha$ emission typical of accretors in the 20-30 Myr old cluster NGC 6167.

Moreover, among the 17 Galactic regions considered in Figure 8 there is a clear outlier, represented as an upside-down triangle: the 16 Myr old Lower Centaurus Crux (LCC)/ Upper Centaurus Lupus (UCL) region, where the typical \dot{M} is higher than expected for its age and is fairly consistent with (though still lower

than) that measured for the 20 Myr old population of NGC 346 in the SMC. Pinzón et al. (2007) presented a comparative study of the average mass accretion rates in Galactic young clusters and associations with ages between 10 and 30 Myr based on photometric excesses in the U band; they already noticed that an important fraction ($\sim 25\%$) of stars in LCC/UCL presents a relative strong accretion. According to these authors, the peculiar case of LCC/UCL might indicate that gas reservoirs in disks can exceptionally exist much longer than 10 Myrs, allowing the formation of giant planets up to the age of ~ 16 Myr (see also Moór et al. 2011). However, no strong correlation was found between U-band excess emission and $H\alpha$ -excess emission for the stars in the LCC/UCL and some doubts arouse about the nature of the U-band excess (R. de la Reza, private communication).

For the sake of clarity, we also point out that the study by Pinzón et al. (2007) finds 8 accretors in Tuc-Hor and 5 in β -Pic in the mass range 1-2 M_{\odot} , while previous studies of the PMS population of these associations (Jayawardhana et al. 2006) find only 2 accretors in β -Pic and none in Tuc-Hor. The authors do not discuss this discrepancy.

In the MCs, we measure an average \dot{M} of $5 \cdot 10^{-8} M_{\odot}/\text{yr}$ for 10-12 Myr old stars, indicating that disks in the MCs might be long-lived with respect to the MW. Observational measurements of the disk lifetime in the LMC and, in general, low-metallicity environments are at the moment very poor and controversial. Using data from the Spitzer SAGE Survey in the MCs, it was found that the fraction of stars with disks in the SMC is higher than in the LMC (D. Lennon, private communication). Being the SMC more metal poor than the LMC, this would be consistent with a

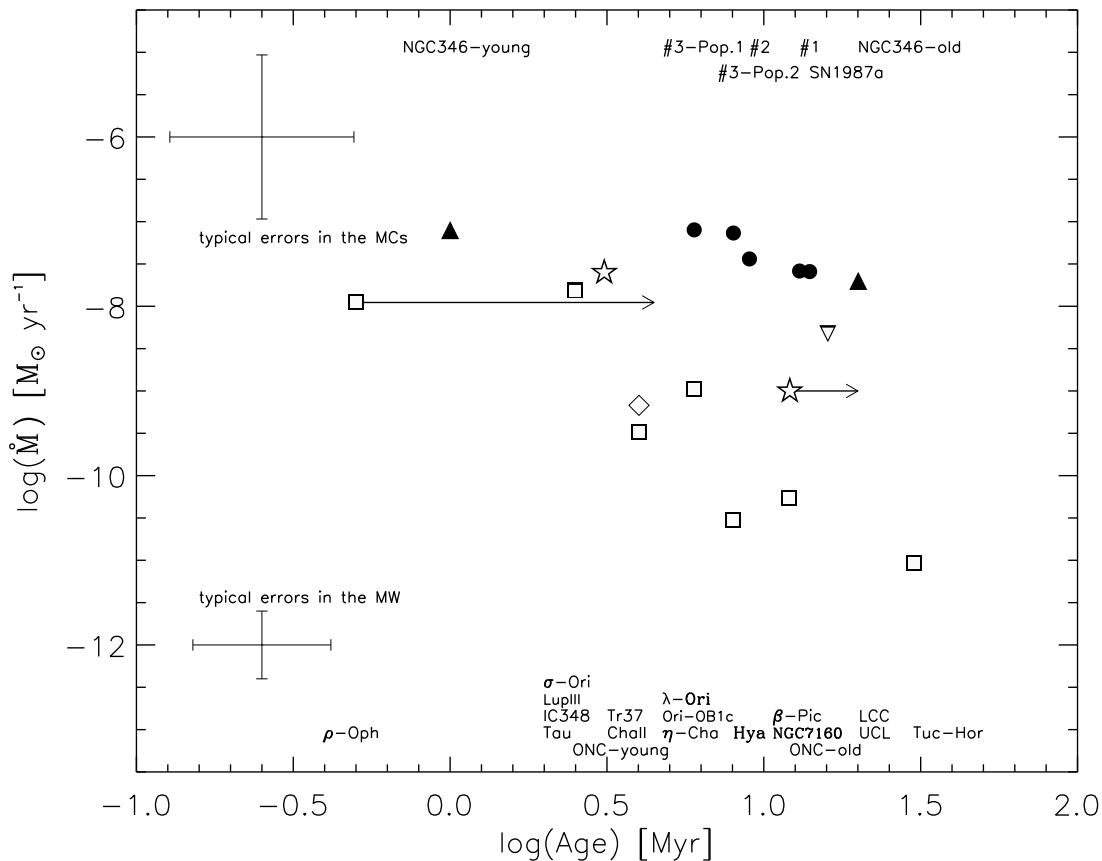


Figure 8. Median mass accretion rate as a function of the median age for PMS populations in the LMC (filled circles) and 17 young clusters and star forming regions in the MW (open squares), as indicated in the labels. The upside-down triangle represents the measurement for the LCC/ UCL region, while the diamond and the pentagrams are the photometric measurements by Barentsen et al. (2011) and Panagia et al. (2011, in preparation), respectively. The arrows indicate the age uncertainty for the ρ -Oph members and the ONC-old population (see Table 5). The typical errors on \dot{M} and age are displayed in the top-left and bottom-left for the MC and MW regions, respectively.

scenario where the disk lasts longer in a metal poorer environment. On the other hand, in the extreme outer Galaxy (EOG), where the metallicity is one-tenth of the solar neighborhood, Yasui et al. (2009) found a fraction of stars with circumstellar disks significantly lower than in the solar neighborhood, suggesting that most stars in low-metallicity environments experience disk dissipation at earlier stages (<1 Myr). The mismatch between these two results is rather awkward. Yasui et al. (2009) might have underestimate the disk fraction in the EOG because their measurements are based only on near-IR excess, which can be very small or inexistent in flattened disks. Moreover, Yasui et al. (2009) warn that a mechanism specific to the EOG environment, i.e. effective far-ultraviolet photoevaporation, might contribute to the rapid disk dispersal (see, e.g., Haywood 2008). The mechanisms of disk dispersal and their dependency on metallicity are further discussed in Sect. 8 to 8.4.2.

6.2 Disk mass

In order to keep an average \dot{M} of $5 \cdot 10^{-8} M_{\odot}/\text{yr}$ for ~ 10 Myr, the disks we are observing in the MCs should be very massive, i.e. about $0.5 M_{\odot}$. Moreover, it is normally assumed that accretion rates are much higher in the protostellar phase (≤ 1 Myr) than at 5-10 Myr. Thus, if it is really true that PMS stars in the LMC have

average \dot{M} of $5 \cdot 10^{-8} M_{\odot}/\text{yr}$ at 10 Myr, one would expect them to have even higher \dot{M} at earlier ages and, hence, even higher disk mass.

Disk properties and initial conditions may be different in low-metallicity environments and disk dispersal mechanisms other than accretion might contribute to dissipating the disk mass. Moreover, a recent study by Zhu et al. (2010) suggests that, if the initial cloud core is moderately rotating, the protostar ends up with a more massive disk and most of the central star's mass is built up during FU Ori-like outburst events of accretion. However, it is still hard to explain how such massive disks are produced, because observations in the MW suggest that stars accrete most of their mass in the embedded phase, and only a few percentage once they reach the T Tauri phase.

The high \dot{M} measured in the MCs would imply that the overall accretion process during the PMS phase will add to the central object a mass comparable to that of the central object itself and, hence, the protostars itself should have as much mass in the central object as in the disk/envelope. This appears unlikely, because the Initial Mass Function (IMF) in the MCs appears remarkably similar to the that of the MW (e.g., Garmany 1998; Bastian et al. 2010).

However, there is an important point to be considered when doing such speculations. The mass accretion process of stars in the PMS phase is a highly variable phenomenon and this vari-

ability is reflected in the diagnostics used to measure \dot{M} ($H\alpha$ excess emission, veiling, mid-IR Br γ and Pa β emission, etc.; Herbst 1986; Hartigan et al. 1991; Nguyen et al. 2009; Fedele et al. 2010; Petrov et al. 2011; Faesi et al. 2011). At any given time, only a certain fraction of PMS stars of the given PMS population shows signatures of mass accretion above the detection limit of the given survey. The study by Fedele et al. (2010), based on $H\alpha$ excess emission measurements, shows that the fraction of PMS stars with \dot{M} above their detection limit in Galactic star forming regions decreases with age. At the typical age of our PMS star candidates (~ 10 Myr), the fraction of PMS stars with \dot{M} above their detection limit is expected to be of the order of 5% (see Figure 3 and 4 by Fedele et al. 2010) or, in other words, their \dot{M} is above the detection limit only for 1/20 of the time.

Since the mass accretion process depends on metallicity (see Sect. 8), this estimate might not be accurate for low-metallicity PMS stars. Indeed, De Marchi et al. (2011c) found that the fraction of PMS stars above their \dot{M} detection limit at ages younger than ~ 10 Myr in the SMC cluster NGC 346 is of the order of 30%. In other words, these PMS stars are above the \dot{M} detection limit only for 1/3 of the time. The metallicity of the LMC is in between the SMC and the MW; we estimate that our PMS star candidates in the LMC, with an average \dot{M} of $5 \cdot 10^{-8} M_{\odot}/\text{yr}$, a typical age of ~ 10 Myr, accrete a total mass of ~ 0.02 up to $\sim 0.2 M_{\odot}$ depending on whether we assume that they are above our \dot{M} detection limit (dashed line in Figure 6) 1/20 or 1/3 of the time. This implies that the disk mass is between 10 and 20% of the stellar mass, because our PMS star candidates have mass in the range 1-2 M_{\odot} , which is plausible (White & Hillenbrand 2004; Alcalá et al. 2008; Kim et al. 2009).

7 CAVEATS ON OUR AGE AND \dot{M} ESTIMATES

As mentioned in Section 3.3, the uncertainty on stellar masses and ages derived from PMS evolutionary models could have a significant impact on our results. In particular, a few caveats on isochronal ages should be taken into account.

Recently Baraffe et al. (2009) showed that, when vigorous episodes of mass accretion at early stages of the stellar life (≤ 1 Myr) are taken into account in the calculation of PMS evolutionary tracks, protostars may have much smaller radii than found in previous treatments. Such small radii would have the effect of making some young stars appear fainter and thus much older in the HR diagram, perhaps as much as 10 Myr, than they really are. This means that the concept of stellar birth-line has no valid support for very low-mass stars because it depends on the accretion history. As a consequence, ages below a few Myr are highly uncertain and absolute ages are hard to determine, though relative ages are still reliable. This problem has a strong impact on \dot{M} evolution studies, because it implies that a strongly accreting object might show a position on the HR diagram consistent with a 10 Myr age, even though its true age is much younger.

However, the prediction by Baraffe et al. (2009) applies to the limit of low-temperature (“cold”) accretion, and Hartmann et al. (2011) argue that very rapid disk accretion is unlikely to be cold, for several reasons: i) the FU Ori objects, e.g. the best-studied PMS disks with rapid accretion outbursts, have spectral energy distributions consistent with large, not small, radii; ii) theoretical models indicate that at high \dot{M} , protostellar disks become internally hot and geometrically thick, making it much more likely that hot material is added to the star; iii) the luminosity of the accretion disk

is likely to irradiate the central star strongly, heating up the outer layers and potentially expanding them. iv) observed HR diagram positions of most young stars are inconsistent with the rapid cold accretion models.

The Baraffe et al. (2009) prediction implies that we might have overestimated the age of our PMS star candidates. This problem affects age estimates both in the MCs and in our MW; however, under the hypothesis that the typical \dot{M} are higher in the MCs, it is expected to be more significant for PMS stars in the MCs. In other words, if we accept a typically higher \dot{M} in the MCs, then we have to accept that our age estimates might be inconsistently derived, because isochronal ages are not robust for strongly accreting objects and we might have overestimated the age of PMS stars in the MCs. This problem can be properly addressed only when improved isochrones for low-metallicity PMS stars will be available. However, this issue does not affect considerably our conclusion based on Figure 8, because the Baraffe et al. (2009) effect is expected to be more significant for very young objects (≤ 1 My) of spectral type M or later, ranging from a few Jupiter masses to a few tenths of a solar mass, while our sample consists essentially of G and K type stars with ages older than ~ 5 My (see Table 4).

Hartmann (2003) discussed the uncertainties in the birth line of G-type stars ($T_{\text{eff}} \gtrsim 5400$ K), which results in an overestimate of their ages and dominate the apparent age spread. We do observe that G-type stars in our sample are systematically older than K-type stars by a few Myr. This age difference is partly explained by the fact that our photometric limits (Table 1) allow us to detect only the brightest and, hence, youngest late K-type stars at the distance of the LMC, while they are sufficient to detect G-type stars of any age and spectral sub-class up to the main sequence (see also Figure 6, upper panel). However, we can not exclude some residual effect due to the uncertainty in the birth line of G-type stars. This would point toward an overestimation of the typical age of PMS populations in the MCs.

Finally, in Sect. 3.3 we pointed out that the regions we are studying are very large, about 100 pc in diameter, and we expect an age dispersion of a few to 10 Myr within each region (Table 4). This age dispersion results from the presence of multiple stellar populations in the same region, which might be the result of sequential and/or triggered star formation (Elmegreen 2000). A typical example in our MW is the Cep OB2 bubble, which is ~ 50 pc in diameter and includes the 12 Myr old cluster NGC 7160, the 4 Myr old Tr 37, the 1 Myr old Tr 37 globule, the 2-3 Myr old Cep B, and several other star formation episodes with ages ranging 1-3 Myr (Patel et al. 1998; Sicilia-Aguilar et al. 2005).

Similarly, the three LMC regions analyzed in this work present a significant age spread. Figure 5 shows the HR diagram for the PMS population of these regions and indicates that they have a typical age of ~ 13 Myr, ~ 9 Myr and 6-8 Myr for region #1, #2 and #3, respectively; however, a small fraction of the PMS population in each region is as young as 1 Myr. Since it is normally assumed that accretion rates are much higher at ages around 1 Myr than at 5-10 Myr (see, e.g., Figure 2 by Sicilia-Aguilar et al. 2010), the median \dot{M} we measure could be driven by the younger populations present in each region. This problem affects also the age and \dot{M} estimates for the MW regions, but it is expected to be less significant because these regions are much smaller.

On the other hand, our conclusion in Sect. 6 are driven by Figure 8 using the median age and \dot{M} of each region in the MCs and the MW. This statistical approach is expected to smoothen the age uncertainty due to strong accretors and/or G-type stars and, indeed, the median isochronal ages estimated for the LMC regions

are supported by several arguments and independent age estimates (Sect. 3.3). However, considering all the caveats listed above, it could be that we are slightly overestimating the age of the MCs regions. Under the most conservative hypothesis that the MC regions are a few Myr younger than our estimates, we still find a systematic and interesting differences between the MCs and the MWs, as the accretion rates in the MCs are about an order of magnitude higher than in Galactic regions of similar age. As we will see in Sect. 8, this difference can be justified on the basis of the different metallicity between the MCs and the MW.

8 MECHANISMS OF DISK DISPERSAL: WHY LOW-METALLICITY DISKS MAY HAVE HIGHER ACCRETION RATES?

Our pioneer study of the mass accretion process in the LMC suggests that disks around metal-poor stars accrete at very high rates with respect to galactic PMS stars with roughly solar metallicity. The many caveats of age/ \dot{M} measurements do not allow us to quantify such a difference with high accuracy. However, all our arguments support a difference of at least an order of magnitude in \dot{M} . Models of disk evolution provide several explanations both for and against this observational evidence. In the next sections we review the interplay among the main mechanisms of this dispersal in low-metallicity environments and in relation to our finding in the LMC.

8.1 Viscous accretion

Viscous accretion is the mechanism by which mass is accreted onto the central star because the transport of angular momentum outward allows disk material to flow radially inward (Hollenbach et al. 2000). In general, a lower metallicity implies a lower disk opacity, lower disk temperature, lower viscosity, and thus longer viscous time (see, e.g., review by Durisen et al. 2007). Therefore, it is expected that low-metallicity stars will undergo significant accretion up to older ages with respect to higher metallicity stars, in general agreement with our measurements in the LMC. However, a few warnings must be taken into account:

(i) According to (Hartmann et al. 2006), in disk around low-mass stars the accretion/viscosity is mainly driven by magneto-rotational instability (MRI), which may be more efficient in low metallicity stars. Indeed, this is the argument used by Yasui et al. (2009) to explain the fact that in the EOG, where the metallicity is one-tenth of the solar neighborhood, the fraction of stars with circumstellar disk is significantly lower, implying a faster disk dispersal. This consideration would go against the long-lived low-metallicity disks hypothesis. Nevertheless, there is no observational evidence that accretion/viscosity driven by MRI is so efficient. For example, evolved disks with large grains, which are expected to behave like low-metallicity disks, accrete less as they age, while, under the assumption that the MRI is more efficient at low-metallicity, we would expect the opposite (see Sect. 5 by Hartmann et al. 2006, and references therein).

(ii) In order to keep an average accretion rate of $10^{-7} M_{\odot}/\text{yr}$ going on for 5-10 Myr, the disks we are observing in the LMC should be extremely massive, about 0.5-1 M_{\odot} . An additional effect to take into account in massive disks is gravitational instability (GI). It has been suggested that lower opacity favor GI (Cossins et al. 2009) and that low metallicity disks may be more unstable against GI (Cai et al. 2006). There is an ongoing debate

about whether GI makes very massive disks fragment (Boss 1997, 2003; Cai et al. 2006, 2009), or simply favor accretion and mass transport (Hartmann et al. 2006). In both cases, the GI global effect would point against the long-lived low-metallicity disk hypothesis, even though it could explain the large \dot{M} we measure.

8.2 Grain growth

According to the analysis by Dullemond & Dominik (2005), the growth of dust particles in the disk depends on the disk's dust to gas ratio. Low-metallicity disks have a lower dust content and, hence, the process is slower and the grains remain small. Grain growth is an important contributing factor to disk dissipation by planet formation and photo-evaporation, which we will analyze later on. In addition, if the disk is less optically thick, the convective turbulence is reduced, making the grain coagulation/fragmentation process less efficient. In other words, low-metallicity disks may reach a quiet steady state characterized by small grains that cannot coagulate and, hence, they last longer, because dissipation by planet formation and/or photo-evaporation is less efficient. This scenario is in agreement with our measurements in the LMC, but again there are a few warnings to take into account:

(i) Convection is not the only source of turbulence. As seen in Sect. 8.1, MRI driven turbulence will be present in the magnetically active parts of the disk. However, the high \dot{M} we measure at older ages suggests large disk mass to sustain such long accretion lifetimes and, hence, a high gas column density. This kind of disks would present magnetically "dead zones" (Turner et al. 2007; Turner & Sano 2008) with lower turbulence. These dead zones might suffer from other types of instability (e.g. streaming instability, Johansen & Youdin 2007) and they may be good locations for planetesimal formation. However, as seen in Sect. 6 and 8.1, such large disk masses are difficult to explain.

(ii) The lower dust content of low-metallicity disk implies that the gas reservoir of the disk is less shielded against photo-evaporation and it might be depleted faster. Disk photo-evaporation effects and their dependency on metallicity are discussed in Sect. 8.4.

8.3 Planet formation

Johansen et al. (2009) presented three dimensional numerical simulations of particle clumping and planetesimal formation in protoplanetary disks with varying amounts of solid material. These simulations showed that the formation of planetesimals is strongly dependent on the dust to gas ratio. Low-metallicity disks would not be able to produce planets at the beginning, but they may do it later on once other mechanisms, like internal photo-evaporation, have reduced the amount of gas. Thus, the correlation between host star metallicity and exoplanets may reflect the early stages of planet formation and low-metallicity disks can be particle enriched during the gas dispersal phase, leading to a late burst of planetesimal formation. The metallicities studied by Johansen et al. (2009) are solar or super-solar, not as low as in the LMC. However, if low-metallicity disks would produce planets only in late phases, they might be able to keep an average \dot{M} higher than higher metallicity disk, because early proto-planet growth might reduce the accretion to the central star (Merín et al. 2010, and references therein). In a very low-metallicity environment such as the LMC, this effect might be enhanced and would explain the large \dot{M} we measure.

For the sake of completeness, we defer the reader to the fol-

lowing works pointing out other open issues and possible bias on the planet-metallicity correlation:

- Yasui et al. (2009) found that most stars in low-metallicity environments experience disk dissipation at earlier stage (<1 Myr) than in the solar neighborhood and argue that this could be one of the major reasons for the strong planet-metallicity correlation (see Sec. 1), because the shorter disk lifetime reduces the time available for planet formation. This result is in disagreement with our measurements for low-metallicity PMS stars in the LMC, whose accretion process appears to last longer than for galactic PMS stars. In Sect. 6, we have seen that the results by Yasui et al. (2009) might suffer incompleteness effects and the rapid disk dispersal in the EOG might be due to effective far-ultraviolet photo-evaporation rather than planet formation. Moreover, Ercolano & Clarke (2010) explored the metallicity dependence of a dispersal mechanism based on planet formation in the core accretion scenario (Ida & Lin 2004) and found opposite results, i.e. planet formation in low-metallicity environments would extend disk lifetime, because the lower metal content implies a smaller amount of dust and, hence, a slower planet formation process. These authors explain the observations in the EOG in the context of a disc dispersal mechanism based on X-ray photo-evaporation from the central star, which operates faster in low metallicity environments (see discussion in Sect. 8.4).

- According to Bouchy et al. (2009), planets formed in lower-metallicity disks would accrete less gas and would not suffer so much migration; thus, they may end up as low-mass planets very hard to detect.

8.4 On the disk dispersal through photo-evaporation

Photo-evaporation of the surface layer of the gas in the disk can be triggered by strong radiation fields generated by nearby OB stars (external photo-evaporation) and/or the radiation field of the central PMS star itself (internal photo-evaporation Hollenbach et al. 2000). These two mechanisms operate very differently and have very different responses to changes in metallicity. Thus, we analyze them separately.

8.4.1 Internal photo-evaporation

Internal photo-evaporation is the mechanism by which radiation from the central source heats the gas in the disk, enabling it to climb up the gravitational potential well and escape. Theoretical studies of the erosion of circumstellar disks around solar-type stars via internal photo-evaporation suggest typical mass loss rates of $\sim 10^{-10} M_{\odot}/\text{yr}$ (Alexander et al. 2006a,b) for photo-evaporation caused by extreme ultra-violet (EUV) radiation and $\sim 10^{-8} M_{\odot}/\text{yr}$ for photo-evaporation caused by X-rays (Owen et al. 2010). Thus, X-rays appear to be much more efficient at driving internal photo-evaporation (see discussion in Ercolano et al. 2009; Ercolano & Owen 2010). Ercolano & Clarke (2010) explored the metallicity (Z) dependence of X-ray mass loss rates and found that X-ray wind rates are higher in lower- Z environments and, consequently, disk lifetimes are shorter. This occurs because heavy elements represent the main source of opacity for X-rays; the low metallicity implies a reduction of the X-ray opacity and, hence, a larger column can be heated by X-rays (see Figure 2 of Ercolano & Clarke 2010) driving a denser wind from deeper down

in the disk³. We find that metal-poor stars in the LMC accrete at very high rates with respect to galactic PMS stars of the same age, which can be explained in the context of the models presented by Ercolano & Clarke (2010). These authors provides preliminary evidence for shorter disk lifetimes at lower metallicities when X-ray driven photo-evaporation is considered as the main disk dispersal mechanism. To a first approximation a disc will be destroyed by photo-evaporation when $\dot{M} = \dot{M}_w(Z)$, where \dot{M} is the accretion rate through the disk and $\dot{M}_w(Z)$ is the X-ray wind rate. Ercolano & Clarke (2010) show that $\dot{M}_w \propto Z^{-0.77}$. This dependency is steep enough to compensate for the about one order of magnitude difference in \dot{M} between the LMC and the MW, because the LMC has about half solar metallicity. Moreover, mass accretion rates at lower metallicity are expected to be higher because the disk viscosity parameter (α_{acc}) is higher at lower Z . In the MRI scenario this occurs because, thanks to the lower X-ray opacity, a larger mass fraction of the disk is ionized and therefore MRI active.

Thus, a disk dispersal scenario based on internal X-ray photo-evaporation is consistent with the idea of higher \dot{M} at lower metallicity.

8.4.2 External photo-evaporation

External photo-evaporation, caused by nearby massive stars, works primarily via FUV heating of the gas in the outer disk and relies on photoelectric heating from dust grains. The most striking example of external photo-evaporation is seen in the proplyds in Orion (Bally et al. 1998, 2000). Linsky et al. (2007) also argued that the ultra-violet (UV) emission and winds of nearby hot stars play an important role in the development of evaporating gaseous globules (Hester et al. 1996) into protostars. External photo-evaporation is difficult to quantify due to a number of uncertainties, including projection effects, and there still is no clear indication of its global effect on PMS populations.

To study the effect of external photo-evaporation on the PMS populations in our fields, we analyze the spatial distribution of the PMS stars and their level of $H\alpha$ luminosity with respect to the distance from the hot OB stars in the field, following the same approach as in Paper I. To identify OB stars in our fields, we used the catalog of UBVI stellar photometry of bright stars across the central 64 deg^2 area of the LMC and the relative extinction map by Zaritsky et al. (2004). We compare the dereddened photometry of these bright stars with the tabulation of absolute magnitudes of OB stars by Wegner (2000), assuming a distance modulus of 51.4 ± 1.2 kpc (Panagia 1991; Panagia et al. 1991). Only hot stars with spectral type earlier than B1 were considered, because cooler stars do not contribute significantly to the ionization (see Table 1 in Paper I). The center of mass of the hot stars in each field was computed using as weight their bolometric luminosity.

Figure 9 shows the spatial distribution of the PMS stars in our LMC fields and the position of the ionizing stars. The center of mass of the ionizing flux is represented in each region by the large square. Symbols of different colors indicate PMS stars with different level of $H\alpha$ luminosity, as indicated in the caption, and the lines display the contours of the $H\alpha$ nebular emission retrieved

³ Note that photo-evaporation driven by EUV or far ultra-violet (FUV) radiation will not give this result. In the case of FUV, the lack of metals and, hence, dust would actually hinder heating although the reduction of opacity is still present (Gorti & Hollenbach 2009), while in the case of EUV radiation the main source of opacity is Hydrogen rather than metals.

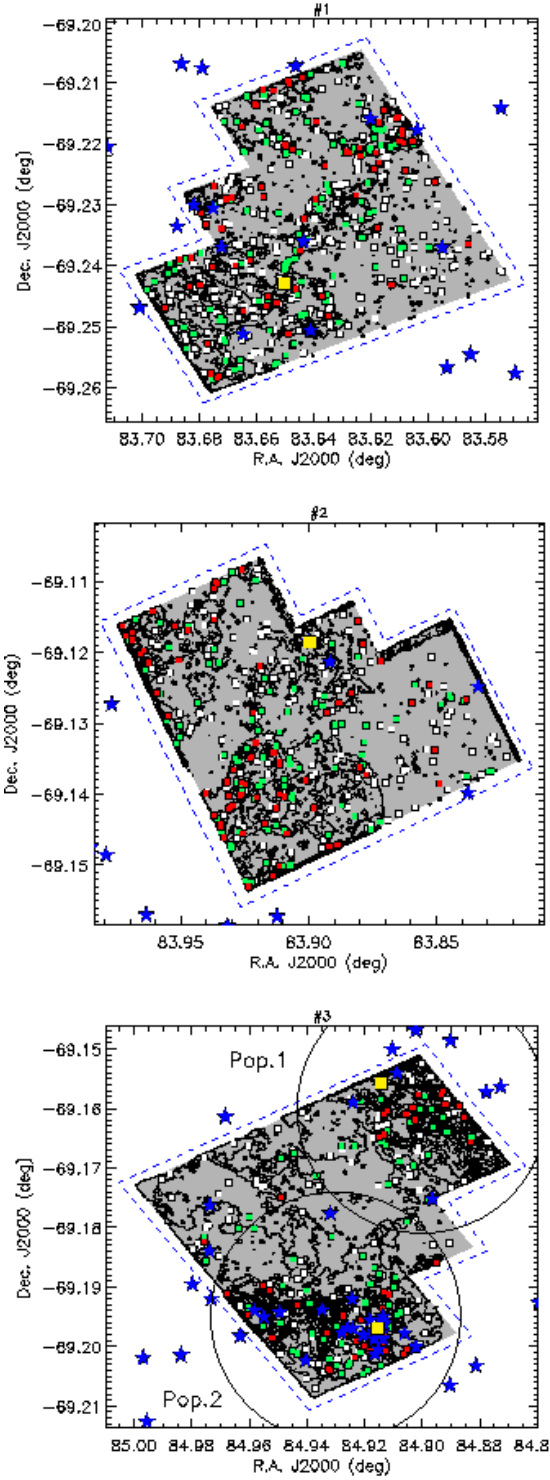


Figure 9. Spatial distribution of the PMS stars in our LMC fields: red squares correspond to PMS stars with $L(H\alpha) > 0.03L_{\odot}$, white squares indicate objects with $L(H\alpha) < 0.01L_{\odot}$, and green diamonds are used for intermediate values. The blue stars indicate the position of the ionizing stars in each field and the large yellow square indicates the relative center of mass. The contours of the $H\alpha$ nebular emission are also drawn (black lines). The two big circles in the lower panel indicate the two possible PMS populations in field #3 and the two yellow squares show the position of the center of mass of the ionizing stars for these two populations.

from our WFPC3/f656n images. Young stars tend to concentrate in region of high dust/gas density and indeed, most of the PMS stars in our sample follow the lanes of the nebular emission. We note, in particular, that our field #3 presents two concentrations of PMS stars corresponding to two well defined over-densities in the nebular emission. Moreover, one of the two groups is also associated to a clear cluster of OB stars. We do not observe a significant age difference between these two groups (Table 4), also because of the limitations in the age determination (Sect. 3.3). However, the peculiar spatial distribution suggests that two populations of PMS stars separated by about 0.035 deg (i.e. ~ 30 pc at the distance of the LMC) might be present in this region, as indicated by the circles in Figure 9. Thus, in our analysis we deal with these two groups separately and refer to them as field #3-Pop.1 and field #3-Pop.2.

Figure 9 shows a variety of behaviors in the spatial distribution and typical $H\alpha$ luminosity of the PMS stars with respect to the center of mass of the OB stars for the three LMC fields. To show this difference quantitatively, we plot in Figure 10 the frequency of PMS stars and their typical $H\alpha$ luminosity as a function of the distance to the closest ionizing OB stars for 5 distance bins. The dashed lines display the linear fit to the points, which gives an indication of the global trend of the data. The same plots have been presented in Paper I for the field around the supernova SN1987A (see their Figure 13 and 14). The result of this analysis for the LMC fields can be summarized as follows.

For the field around supernova SN1987A, we found in Paper I that PMS stars in the vicinity of OB stars are both less numerous and fainter in $H\alpha$ emission than farther away. This suggests that their circumstellar disks have been considerably eroded, and made less efficient, by enhanced photo-evaporation caused by the ionizing radiation of the massive stars integrated over their ~ 2 Myrs lifetime. As shown in Figure 10, we find a similar behavior in our field #3-Pop.1, where the number of PMS star candidates in the vicinity of OB stars is lower than farther away. However, the $H\alpha$ luminosity of this PMS population does not show any specific trend with respect to the position of OB stars.

The inspection of Figure 10 for the PMS population of our field #1 and field #3-Pop.2 shows a different trend. In these two fields there are more PMS stars near the ionizing OB stars, while their typical $H\alpha$ luminosity is roughly constant. These correlations are consistent with a scenario where photo-evaporation due to ionizing radiation of nearby OB stars does not play a significant role for disk dissipation.

Moreover, the fact that the distribution of low-mass stars follows the distribution of massive stars suggests that i) either they belong to the same generation or ii) they formed during separate events of star formations sharing the same center of mass. Regions #1 and #3-Pop.2 are 11 and 6 Myr old, respectively (Table 4); although we could have slightly overestimated the age of these regions (Sect. 7), both of them are too old to assume that the low-mass PMS stars and the OB stars belong to the same generation. Thus, our data support hypothesis ii), i.e. two events of star formation separated by a few Myr might have occurred in these regions. Indication of multiple events of star formation within the same cluster have been already reported in the literature (Patel et al. 1998; Sicilia-Aguilar et al. 2005; Vinkó et al. 2009; Milone et al. 2009; Beccari et al. 2010; De Marchi et al. 2011a).

The inspection of Figure 9 and 10 for field #2 does not reveal any clear trend.

Thus, the LMC stellar populations show a variety of behaviors with respect to disk photo-evaporation due to external radiation fields. Although this result might appear puzzling, there is a

number of considerations which help illustrating the complexity of the problem and understanding the “no trend” detection in field #2. Indeed, even in our Galaxy, it is very common to see disk photo-evaporation effects in individual case (see, e.g., the case of Trumpler 37; Mercer et al. 2009), while finding a “global” trend is much harder for several reasons.

The first reason is purely statistical. Even in a large, massive cluster there will be few objects close enough to the massive stars (~ 1 pc) to significantly suffer photo-evaporation effects. In addition, we can only measure projected distances and this implies that lots of contaminants, that are not as close to the OB stars as we might think, are included in the analysis.

Secondly, low-mass PMS stars need to spend a few Myr within 1-2 pc distance from a OB star to significantly suffer disk photo-evaporation effects, though the timescale of this process is still very uncertain. With a typical dispersion velocity of 1-2 km/s (see, e.g., Kraus & Hillenbrand 2008, and reference therein), many low-mass stars move 1-2 pc per Myr or more if they are ejected and, hence, even if they were originally close to a massive star they may end up somewhere else.

Furthermore, the structure/orientation of the given young cluster can be such that it happens to have another young population in the close foreground/background. This second population is not physically connected with the cluster under study, but it is indistinguishable because we can only measure projected distances. In these cases, any correlation with the position of OB stars would be even harder to detect.

Finally, triggered star formation may mimic the effect of external photo-evaporation. If the winds of a massive stars triggers more star formation in the outskirts of the cluster, as seen in the galactic cluster Tr 37 (Sicilia-Aguilar et al. 2005), the disk fraction is higher at larger distances from the massive star. This occur just because the stellar population there is younger and is not a disk photo-evaporation effect.

Because of these overall uncertainties, we consider it premature to discuss the metallicity dependency of disc dispersal through external photo-evaporation.

9 CONCLUSIONS

We presented a multi-wavelength study of three star forming regions in the LMC spanning the age range 1-14 Myr. We aim at investigating the mass accretion process in an environment with a metallicity significantly lower than our MW. We identify about 1000 PMS star candidates actively undergoing mass accretion in these regions on the basis of their $H\alpha$ emission and estimate their mass, age and mass accretion rate. Our measurements represent the largest \dot{M} dataset for low-metallicity stars presented so far. The conclusions of our study are as follows:

- In the mass range 1-2 M_{\odot} , the \dot{M} of PMS stars in the LMC increases with stellar mass as $\dot{M} \propto M_{\star}^b$ with $b \approx 1$, i.e. slightly slower than the second power law previously reported for galactic PMS stars in the same mass regime, and in agreement with the recent results by Barentsen et al. (2011) for the galactic HII region IC 1396 ($b=1.2-1.3$).
- We find that the typical \dot{M} of PMS stars in the LMC is higher than for galactic PMS stars of the same mass, independently of their age. Considering the caveats of isochronal age and \dot{M} estimates, the typical difference in \dot{M} between the MCs and our MW appear to be about an order of magnitude;

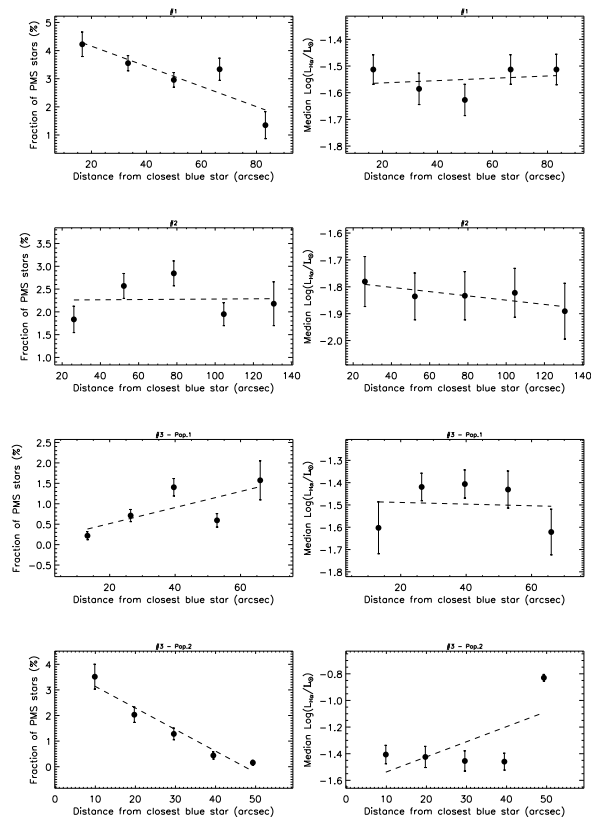


Figure 10. Fraction of PMS stars with respect to all stars (left panels) and relative median $H\alpha$ luminosity (right panels) as a function of the distance from the closest ionizing star for our fields #1, #2 and the two possible PMS populations in field #3 in the LMC. The dashed line in each panel is the linear fit to the points.

- Currently available models of disk evolution/dispersal support the hypothesis that the higher \dot{M} measured in the LMC might be a consequence of its lower metallicity with respect to our MW;
- The sample of PMS populations studied in the LMC shows a variety of behaviors with respect to disk photo-evaporation due to external radiation fields. In the region around supernova SN 1987A (Paper I) we found clear evidence that circumstellar disks have been eroded by photo-evaporation caused by nearby massive stars. In the three regions analyzed in this work, there is no clear evidence of such an effect. However, the analysis of the spatial distribution of the PMS populations in region #1 and #3-Pop. 2 with respect to the massive OB stars in the field revealed signs of sequential star formation.

In order to clarify these issues, improved evolutionary models for low-metallicity PMS stars and modeling/calculations of disk dispersal at low-metallicity are needed, as well as observations of slightly older (e.g. 30-50 Myr) low-metallicity regions than those presented in this paper.

ACKNOWLEDGMENTS

We are grateful to an anonymous referee whose suggestions have helped us to improve the presentation of this work. We thank A. Natta, L. Testi and G. Beccari, for the many useful discussions and suggestions, and M. Romaniello for making available his tool for

calculating stellar masses and ages. This publication makes extensive use of data products from the HST archive at the Canadian Astronomy Data Centre (CADDC), operated by the National Research Council of Canada with the support of the Canadian Space Agency.

REFERENCES

- Adams, F., Hollenbach, D., Laughlin, G., & Gorti, U. 2004, *ApJ*, 611, 360
- Alcalá, J.M., Spezzi, L., Chapman, N., et al. 2008, *ApJ*, 676, 427
- Alexander, R.D., Clarke, C.J., & Pringle, J.E. 2006, *MNRAS*, 369, 216
- Alexander, R.D., Clarke, C.J., & Pringle, J.E. 2006, *MNRAS*, 369, 229
- Bally, J., Sutherland, R. S., Devine, D., & Johnstone, D. 1998, *AJ*, 116, 293
- Bally, J., O'Dell, C. R., & McCaughrean, M. J. 2000, *AJ*, 119, 2919
- Baraffe, I., Chabrier, G., & Gallardo, J. 2009, *ApJ*, 702, 27
- Baggett, S., et al. 2002, in *HST WFPC2 Data Handbook*, v. 4.0, ed. B. Mobasher, Baltimore, STScI
- Barentsen, G., et al. 2011, *MNRAS*, 415, 103
- Bastian, N., Covey, K. R., & Meyer, M. R. 2010, *Ann. Rev. A&A*, 48, 339
- Baume, G., Carraro, G., Comeron, F., & de Elía, G. C. 2011, *A&A*, 531, A73
- Beccari, G., et al. 2010, *ApJ*, 720, 1108
- Bertin, E., & Arnouts, S. 1996, *A&A Supp.*, 117, 393
- Bessel, M.S., Castelli, F., & Plez, B. 1998, *A&A*, 333, 231
- Bopp, B.W., & Schmitz, M., 1978, *PASP*, 90, 531
- Boss, A. P. 1997, *Science*, 276, 1836
- Boss, A. P. 2003, *ApJ*, 599, 577
- Bouchy, F., et al. 2009, *A&A*, 496, 527
- Cai, K., Durisen, R. H., Michael, S., Boley, A. C., Mejía, A. C., Pickett, M. K., & D'Alessio, P. 2006, *ApJL*, 636, L149
- Cai, K., Durisen, R. H., & Zhu, Z. 2009, *Bulletin of the American Astronomical Society*, 41, #439.01
- Calvet, N., Hartmann, L., & Strom, E. 2000, in "Protostars and Planets", eds V. Mannings, A. Boss, S. Russell (Tucson: University of Arizona Press), 377
- Calvet, N., Muzerolle, J., Briceño, C., Hernández, J., Hartmann, L., Saucedo, J. L., & Gordon, K. D. 2004, *AJ*, 128, 1294
- Clarke, C. & Pringle, J. 2006, *MNRAS*, 370, L10
- Cossins, P., Lodato, G., & Clarke, C. J. 2009, *MNRAS*, 393, 1157
- Dahm, S. 2008, *AJ*, 136, 521
- Da Rio, N., Gouliermis, D. A., & Gennaro, M. 2010, *ApJ*, 723, 166
- De Marchi, G., Panagia, N., & Romaniello, M. 2010, *ApJ*, 715, 1 (Paper I)
- De Marchi, G., Panagia, N., Romaniello, M., Sabbini, E., Sirianni, M., Prada Moroni, P. G., & Degl'Innocenti, S. 2011, arXiv:1104.4494 (Paper II)
- De Marchi, G., et al. 2011, arXiv:1106.2801
- De Marchi, G., Panagia, N., & Sabbini, E. 2011, arXiv:1106.5780
- Dullemond, C. P., & Dominik, C. 2005, *A&A*, 434, 971
- Durisen, R. H., Boss, A. P., Mayer, L., Nelson, A. F., Quinn, T., & Rice, W. K. M. 2007, *Protostars and Planets V*, 607
- Elmegreen, B. G. 2000, *ApJ*, 530, 277
- Ercolano, B., Clarke, C. J., & Drake, J. J. 2009, *ApJ*, 699, 1639
- Ercolano, B., & Clarke, C.J., 2010, *MNRAS*, 402, 2735
- Ercolano, B., & Owen, J. E. 2010, *MNRAS*, 406, 1553
- Esteban, C., & Peimbert, M. 1995, *Revista Mexicana de Astronomía y Astrofísica Conference Series*, 3, 133
- Faesi, C., Covey, K. R., Gutermuth, R., et al. 2011, *Bulletin of the American Astronomical Society*, 43, #340.32
- Fang, M., van Boekel, R., Wang, W., et al. 2009, *A&A*, 504, 461
- Fedele, D., van den Ancker, M.E., Henning, T., Jayawardhana, R., & Oliveira, J.M., 2010, *A&A*, 510, A72
- Fischer, D.A., & Valenti, J. 2005, *ApJ*, 622, 110
- Fitzpatrick, E. L., & Savage, B. D. 1984, *ApJ*, 279, 578
- Garmany, C. D. 1998, *Origins*, 148, 184
- Gonzalez, G. 1997, *MNRAS*, 285, 403
- Gorti, U., & Hollenbach, D. 2009, *ApJ*, 690, 1539
- Gullbring, E., Hartmann, L., Briceño, C., & Calvet, N. 1998, *ApJ*, 492, 323
- Haisch, K.E., Lada, E.A., & Lada, C.J. 2001, *ApJ*
- Hartigan, P., Kenyon, S.J., Hartmann, L., et al. 1991, *ApJ*, 382, 617
- Hartmann, L., Calvet, P., Gullbring, E., D'Alessio, P. 1998, *ApJ*, 495, 385
- Hartmann, L., 2003, *ApJ*, 585, 398
- Hartmann, L., D'Alessio, P., Calvet, N., & Muzerolle, J. 2006, *ApJ*, 648, 484
- Hartmann, L., Zhu, Z., & Calvet, N. 2011, arXiv:1106.3343
- Harvey, P., Merín, B., Huard, T.L., et al. 2007, *ApJ*, 663, 1149
- Haywood, M. 2008, *A&A*, 482, 673
- Herbig, G. H. 1960, *ApJs*, 4, 337
- Herbst, W., 1986, *PASP*, 98, 1088
- Herczeg, G.J., & Hillenbrand, L.A., 2008, *ApJ* 681, 594
- Hester, J.J., Scowen, P.A., Sankrit, R., et al. 1996, *AJ*, 111, 2349
- Hollenbach, D.J., Yorke, H.W., & Johnstone, D. 2000, *Protostars and Planets IV*, 401
- Ida, S., & Lin, D. N. C. 2004, *ApJ*, 616, 567
- Isella, A., Carpenter, J.M., & Sargent, A.I., 2009, *ApJ*, 701, 260
- Jayawardhana, R., Coffey, J., Scholz, A., et al. 2006, *ApJ* 648, 1206
- Jeffries, R. D. 2011, arXiv:1102.4752
- Johansen, A., & Youdin, A. 2007, *ApJ*, 662, 627
- Johansen, A., Youdin, A., & Mac Low, M.-M. 2009, *ApJL*, 704, L75
- Kenyon, S. J., & Hartmann, L. 1995, *ApJS*, 101, 117
- Kim, K. H., et al. 2009, *ApJ*, 700, 1017
- Kraus, A. L., & Hillenbrand, L. A. 2008, *ApJL*, 686, L111
- Linsky, J.L., Gagné, M., Mytyk, A., et al. 2007, *ApJ*, 654, 347
- Maeder, A., Grebel, E.K., & Mermilliod, J.-C. 1999, *A&A*, 346, 459
- Marcy, G. W., & Butler, R. P. 1998, *Ann. Rev. A&A*, 36, 57
- Marigo, P., Girardi, L., Bressan, A., et al. 2008, *A&A*, 482, 883
- Mayne, N. J., Naylor, T., Littlefair, S. P., Saunders, E. S., & Jeffries, R. D. 2007, *MNRAS*, 375, 1220
- Mayor, M., & Queloz, D. 1995, *Nature*, 378, 355
- Mercer, E. P., Miller, J. M., Calvet, N., Hartmann, L., Hernandez, J., Sicilia-Aguilar, A., & Gutermuth, R. 2009, *AJ*, 138, 7
- Merín, B., Jorgensen, J., Spezzi, L., et al. 2008, *ApJS*, 177, 551
- Merín, B., et al. 2010, *ApJ*, 718, 1200
- Milone, A.P., Bedin, L.R., Piotto, G., & Anderson, J., 2009, *A&A*, 497, 755
- Mohanty, S., Basri, G., & Jayawardhana, R. 2005, *Astronomische Nachrichten*, 326, 891
- Moór, A., Ábrahám, P., Juhász, A., et al. 2011, arXiv:1109.2299
- Muzerolle, J., Calvet, N., Briceño, C., Hartmann, L., & Hillenbrand, L. 2000, *ApJ*, 535, L47

- Muzerolle, J., Luhman, K., Briceño, C., Hartmann, L. & Calvet, N. 2005, *ApJ*, 625, 906
- Natta, A., Testi, L., Muzerolle, J., Randich, S., et al. 2004, *A&A*, 424, 603
- Natta, A., Testi, L., & Randich, S. 2006, *A&A*, 452, 245
- Nguyen, D.C., Scholz, A., van Kerkwijk, M.H., et al. 2009, *ApJ*, 694, L153
- Owen, J. E., Ercolano, B., Clarke, C. J., & Alexander, R. D. 2010, *MNRAS*, 401, 1415
- Padgett, D. 1996, *ApJ*, 471, 847
- Panagia, N. 1991, in "New Views of the Magellanic Clouds", IAU Symp. 190, eds. Y.-H. Chu, N. Suntzeff, J. Hesser, D. Bohlender (San Francisco: ASP), 549
- Panagia, N., Gilmozzi, R., Macchetto, F., Adorf, H.-M. & Kirshner, R. P. 1991, *ApJ*, 380, L23
- Panagia, N., Romaniello, M., Scuderi, S. & Kirshner, R. 2000, *ApJ*, 539, 197
- Patel, N. A., Goldsmith, P. F., Heyer, M. H., Snell, R., & Pratap, P. 1998, IAU Colloq. 166: The Local Bubble and Beyond, 506, 42
- Petrov, P. P., Gahm, G. F., Stempels, H. C., Walter, F. M., & Artemenko, S. A. 2011, arXiv:1109.1266
- Pinzón, G., de la Reza, R., Torres, C.A.O., Seifahrt, A., Neuhauser, R., Proceedings of the *IAU Symposium 243 - Star-disk interaction in young stars*, Grenoble, 21-25 May, 2007
- Rigliaco, E., Natta, A., Randich, S., Testi, L., & Biazzo, K. 2011, *A&A*, 525, A47
- Romaniello, M. 1998, PhD thesis, Scuola Normale Superiore, Pisa, Italy
- Romaniello, M., Panagia, N., Scuderi, S. & Kirshner, R. 2002, *AJ*, 123, 9157
- Salpeter, E. E. 1955, *ApJ*, 121, 161
- Santos, N.C., Israelian, G., Mayor, M., Rebolo, R., & Udry, S. 2003, *A&A*, 398, 363
- Santos, N. C., Mayor, M., Bouchy, F., Pepe, F., Queloz, D., & Udry, S. 2007, *A&A*, 474, 647
- Scuderi, S., Panagia, N., Gilmozzi, R., Challis, P. & Kirshner, R. 1996, *ApJ* 465, 956
- Setiawan, J., et al. 2003, *A&A*, 398, L19
- Setiawan, J., Klement, R. J., Henning, T., Rix, H.-W., Rochau, B., Rodmann, J., & Schulze-Hartung, T. 2010, *Science*, 330, 1642
- Sicilia-Aguilar, A., Hartmann, L., Hernandez, J., Briceño, C., Calvet, N. 2005, *AJ*, 130, 188
- Sicilia-Aguilar, A., Hartmann, L.W., Furesz, G. et al. 2006, *AJ*, 132, 2135
- Sicilia-Aguilar, A., Henning, T., & Hartmann, L.W., 2010, *ApJ*, 710, 597
- Skrutskie, M.F., Cutri, R.M., Stiening, R. et al. 2006, *AJ*, 131, 1163
- Spezzi, L., Alcalá, J.M., Covino, E., et al. 2008, *ApJ*, 680, 1295
- Tognelli, E., Prada Moroni, P. G., & Degl'Innocenti, S. 2011, arXiv:1107.2318
- Turner, N. J., Sano, T., & Dziourkevitch, N. 2007, *ApJ*, 659, 729
- Turner, N. J., & Sano, T. 2008, *ApJ*, 679, L131
- Vinkó, J., Sárneczky, K., Balog, Z., et al., 2009, *ApJ*, 695, 619
- Yasui, C., Kobayashi, N., Tokunaga, A.T., Saito, M., & Tokoku, C., *ApJ*, 705, 54
- Waters, L. B. F. M., & Waelkens, C. 1998, *Ann. Rev. A&A*, 36, 233
- Wegner, W. 2000, *MNRAS*, 319, 771
- White, R.J., & Basri, G. 2003, *ApJ*, 582, 1109
- White, R., & Hillenbrand, L. 2004, *ApJ*, 616, 998
- Wilking, B. A., Gagné, M., & Allen, L. E. 2008, *Handbook of Star Forming Regions*, Volume II, 351
- Worden, S.P., & Peterson, B.M., 1976, *ApJ*, 206, L145
- Zaritsky, D., Harris, J., Thompson, I.B., & Grebel, E.K. 2004, *AJ*, 128, 1606
- Zhu, Z., Hartmann, L., & Gammie, C. 2010, *ApJ*, 713, 1143

This paper has been typeset from a $\text{\TeX}/\text{\LaTeX}$ file prepared by the author.

